

# Neurogenetic Heterochrony in Chick, Lizard, and Rat Mapped with Wholemount Acetylcholinesterase and the Prosomeric Model

José A. Amat<sup>a</sup> Margaret Martínez-de-la-Torre<sup>b</sup> Carmen María Trujillo<sup>c</sup>  
Bárbara Fernández<sup>b</sup> Luis Puelles<sup>b</sup>

<sup>a</sup>Columbia University, Irving Medical Center, Dept. Psychiatry (Child and Adolescent Psychiatry), New York, NY, USA;

<sup>b</sup>University of Murcia, Dept. Human Anatomy, IMIB-Arrixaca Institute for Biomedical Research, El Palmar, Spain;

<sup>c</sup>Department of Biochemistry, Microbiology, Cell Biology and Genetics, Faculty of Sciences, School of Biology, University of La Laguna, La Laguna, Spain

## Keywords

Neurogenesis · Forebrain · Hindbrain · Acetylcholinesterase · Gradients · Prosomeric model · Vertebrates · Sauropsids · Mammals

## Abstract

In the developing brain, the phenomenon of neurogenesis is manifested heterotopically, that is, much the same neurogenetic steps occur at different places with a different timetable. This is due apparently to early molecular regionalization of the neural tube wall in the anteroposterior and dorsoventral dimensions, in a checkerboard pattern of more or less deformed quadrangular histogenetic areas. Their respective fate is apparently specified by a locally specific combination of active/repressed genes known as “molecular profile.” This leads to position-dependent differential control of proliferation, neurogenesis, differentiation, and other aspects, eventually in a heterochronic manner across adjacent areal units with sufficiently different molecular profiles. It is not known how fixed these heterochronic patterns are. We reexamined here comparatively early patterns of forebrain and hindbrain neurogenesis in a lizard (*Lacerta galloti*),

a bird (the chick), and a mammal (the rat), as demonstrated by activation of acetylcholinesterase (AChE). This is an early marker of postmitotic neurons, which leaves unlabeled the neuroepithelial ventricular cells, so that we can examine cleared wholemounts of the reacted brains to have a birds-eye view of the emergent neuronal pattern at each stage. There is overall heterochrony between the basal and alar plates of the brain, a known fact, but, remarkably, heterochrony occurs even within the precocious basal plate among its final anteroposterior neuromeric subdivisions and their internal microzonal subdivisions. Some neuromeric units or microzones are precocious, while others follow suit without any specific spatial order or gradient; other similar neuromeric units remain retarded in the midst of quite advanced neighbors, though they do produce similar neurogenetic patterns at later stages. It was found that some details of such neuromeric heterochrony are species-specific, possibly related to differential morphogenetic properties. Given the molecular causal underpinning of the updated prosomeric model used here for interpretation, we comment on the close correlation between some genetic patterns and the observed AChE differentiation patterns.

© 2022 S. Karger AG, Basel

## Introduction

Developmental *heterochrony* refers to comparable mechanisms or patterns of development that occur displaced in relative time. It applies to phylogeny, when comparing different species in evolutionary context, but also to ontogeny, when *the same process or pattern occurs at different ontogenetic times* at different positions (e.g., in the brain). The latter use accordingly examines ontogenetic *heterotopic heterochrony* (position-related temporal displacement of a particular developmental process). The embryonic brain shows many instances of heterotopic heterochrony due to its complex *anteroposterior* and *dorsoventral* regionalization into areal neuroepithelial progenitor domains (called *fundamental morphogenetic units*) [Nieuwenhuys and Puelles, 2016; Nieuwenhuys, 2017]. It is common knowledge now that each of these has an unique developmental molecular profile that leads them to regulate independently their proliferative and differentiative processes according to the local combination of active/inactive genes. Sharing of significant genes among adjacent serially transverse morphogenetic units apparently underlies metameric repeating of an histogenetic pattern along a series of units (e.g., forming plurisegmental patterns that generate multimodular sensory columns) [Marin et al., 2008; Puelles, 2013; Tomás-Roca et al., 2016]. Examined across species, the map of molecularly defined brain fundamental morphogenetic units is known to show considerable evolutionary conservatism, defining the so-called *ontogenetic brain Bauplan*. In this, fixed component units may vary in relative size and observable histogenetic properties over time but keep their neighbors or topologic boundaries. It is less clear whether the *heterochronic neuronal differentiation patterns* are also stereotyped across the shared Bauplan, irrespective of the fact that the speed and length of development may change in different species.

The present research examines heterochronic spatial patterns in the topology of emerging acetylcholinesterase (AChE)-positive young postmitotic neurons in the sauropsidian (chick and lizard) and mammalian (rat) forebrain and hindbrain. We will reexamine and partly reinterpret previously published chick and rat material [Puelles et al., 1987a, 2015a], adding unpublished chick forebrain and rat hindbrain results from Amat's [1986] doctoral thesis, and including as well some hitherto unpublished results from our AChE studies on lizard embryos, done in collaboration with C.M. Trujillo. Emphasis will be placed on the chicken pattern.

The present work reflects a talk on “neurogenetic heterochrony” given at the Karger Symposium in 2020. Our comparative embryonic AChE material was interpreted within the updated prosomeric model [Puelles et al., 2012a; Puelles, 2013; Puelles and Rubenstein, 2015; Puelles, 2018], thus correcting some errors found in our previous publications.

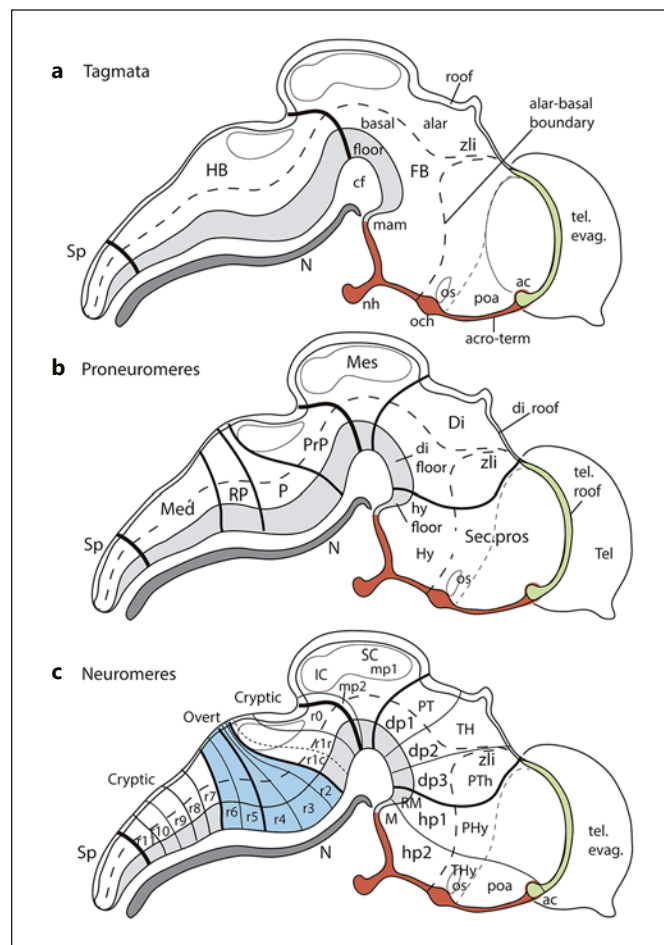
The Puelles et al. [1987a] study of chicken early whole-mount patterns of AChE-labeled newborn neurons employed a then completely heterodox *neuromeric approach* which was largely based on the previous neuromeric embryologic work of von Kupffer [1906], Palmgren [1921], Rendahl [1924], Bergquist and Kallen [1953, 1954], Coggeshall [1964], Vaage [1969, 1973], Keyser [1972], and Gribnau and Geijberts [1985].

This original model was largely developed by the so-called “Nordic school,” though there were earlier cogent notions on neuromeres since Orr [1887] (work on lizard embryo brains). Except for the German von Kupffer, the authors cited above worked in Sweden, Norway, Denmark, and Holland (thus the “Nordic school”); they apparently were directly or indirectly inspired by the Swedish comparative brain histologist and embryologist Niels Holmgren, who supervised the theses of Palmgren, Rendahl, and Bergquist, among others. However, they all tended to work independently [Källén, personal communication to L.P. in 2002]. This model was tentatively applied to diencephalic development by L.P. as of 1977 due to previous failure to explain various sorts of developmental Golgi and AChE data using the standard columnar model of Herrick [1910, 1933, 1948] and Kuhlenbeck [1973].

The slightly modified version of the Nordic neuromeric model offered in Puelles et al. [1987a] was the immediate antecedent of the now well-known *prosomeric model*, produced subsequent to a complementary gene mapping approach in mouse embryos done in collaboration by L.P. and J.L.R. Rubenstein since 1992 [Bulfone et al., 1993; Puelles and Rubenstein, 1993; Rubenstein et al., 1994; Bulfone et al., 1995; Shimamura et al., 1995; Puelles, 1995]. This model was soon tested in amniote and anamniote model vertebrates including agnatha [Pombal et al., 2009], as well as the cephalochordate *Amphioxus* [Albuixech-Crespo et al., 2017]. In the latter species a number of brain Bauplan components normally present in vertebrates are underdeveloped or absent.

Updates of the prosomeric model later appeared in Puelles and Rubenstein [2003], Puelles et al. [2004, 2012a, b], Puelles [2001, 2013], Puelles and Rubenstein [2015], and Puelles [2018]. These molecular studies logically em-

**Fig. 1.** Schemata illustrating three stages in progressive anteroposterior subdivision of the updated prosomeric model. Red = acro-terminal domain; green = prospective telencephalic roofplate; blue = hindbrain central field where the overt rhombomeres r2–r6 are seen; light gray = floorplate; dark gray = notochord. **a** Earliest division into forebrain, hindbrain, and spinal cord *tagmata*. The transverse isthmic boundary separating the forebrain and hindbrain tagmata is drawn as a double-thick black line. **b** Subsequent *proneuromere* subdivisions of the forebrain and hindbrain tagmata; the *forebrain tagma* divides into secondary prosencephalon (including hypothalamus, telencephalon and optic vesicle), diencephalon, and midbrain proneuromeres; the *hindbrain tagma* divides into prepontine, pontine, retropontine, and medullary proneuromeres. The added dividing boundaries are marked as thick black lines. **c** Final neuromeric subdivisions of the proneuromeres. There are hypothalamo-telencephalic prosomeres hp1 and hp2 (SP), diencephalic prosomeres dp1–dp3, and midbrain prosomeres (mesomeres) m1 and m2, all delimited by thin black transverse boundaries orthogonal to the longitudinal zones. In the hindbrain there appear prepontine rhombomeres r0 and r1, pontine units r2–r4, retropontine rhombomeres r5 and r6, and medullary units r7–r11. The schema also indicates which rhombomeres are overt or cryptic, all of them being functionally equivalent. Regionalization increases merely by addition of novel boundaries, always keeping the earlier ones. Note that embryos at the tagmatic or proneuromeric stages do not have the shape shown in the schemata **a** and **b** (copied from **c**), being much smaller and simpler; these schemata, so to speak, emphasize the respective fates.



phasized the description of given gene expression domains consistent with a neuromeric interpretation, providing evidence for a molecularly and causally underpinned Bauplan of the neuraxis, rather than delving on the epiphenomenal neuronal differentiation patterns.

### The Updated Prosomeric Model

The prosomeric model has evolved in recent years, particularly in its hypothalamo-telencephalic and hindbrain parts, and has become better substantiated molecularly and experimentally than the simpler model used by Puelles et al. [1987a].

The axial dimension of the neural tube is defined first. Five universal longitudinal zones of reference are present in all vertebrate brains: (1) the *floorplate* (which is induced up to a rostral end under the mamillary area by the axial notochord [Puelles et al., 2012b; Puelles and Rubenstein, 2015; Puelles, 2018], (2) the *roofplate* (resulting from the median fusion of the medullary folds limiting

peripherally the initial neural plate primordium); its rostral end lies at the anterior commissure [Puelles et al., 1987b; Cobos et al., 2001], (3) the *molecular alar-basal boundary* (which emerges throughout the neural tube due to an early equilibrium generated by antagonistic dorsoventral interplay of ventralizing floor morphogens against dorsalizing roof morphogens [see Puelles et al., 2012a; Puelles and Rubenstein, 2015; Puelles, 2018]. These first three longitudinal landmarks of the neural wall form at three different dorsoventral positions, and we understand now fairly well their causal mechanisms. They are roughly parallel to each other, and, moreover, they co-define the equally longitudinal but wider (4) *basal plate* and (5) *alar plate* of the lateral wall, where most neurogenesis occurs (Fig. 1a).

The rostral end of this quintuple system of longitudinal zones reaches what Puelles et al. [2012a] first called the *acroterminal domain* of the forebrain (this concept was not available before). This is a transverse *linear* ros-

tral end of the neural tube primordium. Indeed, the acroterminal domain has a *ventrodorsal* extent, and reaches from the front of the mamillary body (rostralmost floor) along the rostromedian left-right continuity of the basal and alar plates up to the anterior commissure, the rostralmost roof (acro-term; Fig. 1a). Interestingly, the acroterminal domain is selectively labeled in the mouse at E11.5, E13.5, and E15.5 by the gene *Dlk1* (Allen Developing Mouse Brain Atlas; see our Fig. 15a). The acroterminal territory apparently owes part of its singular properties to its unique reception of strong inductive effects from the *prechordal plate* from early gastrulation stages onwards. The latter is represented by an early axial cell population of the anterior visceral endoderm. The initial static endodermal prechordal plate adheres to the neural ectoderm at the level of the prospective infundibular/tuberal hypothalamus; subsequently some prechordal plate cells undergo an epithelio-mesenchymal transformation and migrate dynamically *dorsalwards* in front of the acroterminal domain, moving from its floor to its roof levels [see Diaz and Puelles, 2020]. The right and left longitudinal alar-basal boundaries clearly meet at the acroterminal domain under the optic chiasma. It has been postulated [Puelles et al., 2012a; Ferran et al., 2015; Puelles, 2017; Diaz and Puelles, 2020] that the dynamic (migrating) prechordal plate cells plus the static acroterminal domain jointly represent the true source of *anteroposterior patterning signals* in the closed neural tube (rather than the anterior neural ridge emphasized by literature, since the latter is a *roof plate locus*, and therefore should have *dorsalizing* morphogenetic effects).

The updated prosomeric model next postulates a series of transverse (anteroposterior) segments of the neural tube observable caudal to the acroterminal domain and always *topologically orthogonal* to the five longitudinal zones. Typically, such AP brain parts extend from the floor to the roof of the neural tube, and thus enclose parts of all the dorsoventral longitudinal zones (establishing a metameric DV structural pattern) [Puelles and Rubenstein, 1993, 2003]. Depending of the developmental stage we may describe AP divisions as tagmata, proneuromeres, or neuromeres (Fig. 1a–c) [Puelles, 2018]. In this work, we will discuss neurogenetic heterochrony in the forebrain and hindbrain tagmata. After growth and further AP patterning, three major parts of the forebrain tagma are delimited as *proneuromeres* (Fig. 1b), namely the *secondary prosencephalon* (SP; hypothalamus plus telencephalon and eyes), the *diencephalon* (Di), and the *midbrain* (Mes). All three share details of dorsoventral patterning and there is evidence for their joint neural induc-

tion by signals from the early node. With continuing anteroposterior growth and regionalization, these *proneuromeres* divide each into *neuromeres* (Fig. 1c).

The secondary prosencephalon divides into two *hypothalamo-telencephalic prosomeres* (hp1, hp2; defined in caudorostral order; Fig. 1c; the hypothalamic portions of these neuromeres are named *peduncular* and *terminal hypothalamus*, respectively – PHy, THy) [Puelles et al., 2012a]. The diencephalon divides into three *diencephalic prosomeres* dp1–dp3 (defined in caudorostral order; often referred to as p1–p3). These contain in their alar domains, respectively, the primordia of the *pretectum* (PT), the *thalamus* (TH; plus epithalamus), and the *prethalamus* (PTh).

Finally, the midbrain divides into a massive rostral *m1 mesomere* (or mp1 midbrain prosomere) and a slender caudal *m2 mesomere* (or mp2; note their *rostrocaudal* order; Fig. 1c). The m1 contains most well-known midbrain structures like the oculomotor nucleus (3), red nucleus, and the superior and inferior colliculi (SC, IC). The tiny m2 mesomere is one of the least known parts of the brain; its existence as an atrophic domain was first postulated by Palmgren [1921; see also Vaage, 1969, 1973], but it was modernly found to have specific derivatives and a differential molecular profile [Hidalgo-Sánchez et al., 2005; Puelles et al., 2012b; Puelles, 2013].

The hindbrain tagma divides first into prepontine, pontine, retropontine, and medullary proneuromeres (PrP, P, RP, Med; Fig. 1b); these subdivide later into 12 rhombomeres (r0–r11; defined in rostrocaudal order; Fig. 1c). The *PrP* (or isthmocerebellar hindbrain) produces r0 and r1 (the latter can be subdivided into rostral and caudal parts), *the P* r2–r4, *the RP* r5 and r6, and the *Med* r7–r11 [see also Puelles et al., 2013]. Some of these rhombomeres – r2–r6 – are referred to as “overt” (meaning they are delimited by visible outer constrictions) and others – r0–r1; r7–r11 – as “cryptic” (no outer constrictions, but with demonstrable equivalent molecular limits) [Marín and Puelles, 1995; Cambroner and Puelles, 2000; Marín et al., 2008; Tomas-Roca et al., 2016].

Our present analysis reexamines heterochronic differentiation patterns in the chick forebrain and hindbrain more extensively than before in the light of the updated prosomeric model and its checkerboard pattern of AP/DV subdivisions considered as fundamental morphogenetic units, adding a glance at corresponding patterns in the lizard and rat forebrain. Shared heterochronic aspects in the developmental appearance of AChE-positive young neurons observed in the three studied amniote species are clearly consistent with the updated prosomeric model

conceived as representing an evolutionarily conserved Bauplan. Such histogenetic Bauplan is held to be underpinned by an evolutionarily conserved system of neuromeric units, comparable delimiting and characterizing gene expression patterns, and related conserved patterning mechanisms throughout vertebrates [Albuixech-Crespo et al., 2017]. Nevertheless, subtle variations of heterochronic pattern were noted between the amniote species studied, which we think may underlie species-specific variant morphogenesis.

## Material and Methods

Chick embryos were incubated at 37.8°C in a rotating forced-draft incubator (eggs obtained from a commercial source). This study comprises chick embryo data between stages HH11 and HH26. The specimens were first collected in saline solution, staged [Hamburger and Hamilton, 1951], and transferred into cold fixative solution (10% formaldehyde in 0.1 M, pH 7.2–7.4 phosphate buffer, with 1 mL of stock 0.5% CaCl<sub>2</sub> solution per 100 mL). Fixation at 4°C varied between 1 h and 24 h (according to size) without significant change in AChE activity.

The size of the pieces was reduced before histochemistry in order to aid penetration of the histochemical reactives. The youngest embryos (stages 9–12) were incubated whole. Between stages 13 and 18 we separated the forebrain, cutting at the isthmus, as well as the spinal cord. The eye vesicles were discarded in most embryos. Additionally, the forebrains were divided into halves, and the covering skin and mesenchyme were dissected away using fine-tipped watchmaker forceps and sharpened tungsten needles. The limit of the wholemount method occurred after stage 26, when the thickest tissue parts showed at their center a whitish patch devoid of histochemical reaction.

After a washing in distilled water or maleate buffer, the neural tube pieces were incubated at 4°C in the medium of Karnovsky and Roots [1964] with acetylthiocholine in acetate buffer at pH 6. The medium contained 8×10<sup>-5</sup> M iso-OMPA, to inhibit pseudo-cholinesterase. Incubation proceeded inside a refrigerator for 8–24 h (or longer, in the largest specimens), with occasional stirring. Controls incubated in the presence of 5×10<sup>-5</sup> M BW284C51 or 10<sup>-5</sup> M physostigmine were negative. Alternative incubation with butyrylthiocholine as a substrate yielded no significant reaction product.

Detailed study and photographic reproduction usually required that all tissues external to the neural primordium (mesenchyme, meninges) be dissected away while submerged in buffer or saline solution. We used the concavity of a Maximow culture slide to contain the fluid, placing the slide on an operating microscope equipped with an underlying light source (visualizing in this way by transparency the reaction product). An electrolytically sharpened and L-bent tungsten needle fixed to the tip of a Pasteur pipette with molten paraffine, jointly with a fine-tipped watchmaker forceps (for holding the tissue), were used to finish these dissections. After the end of this process, the specimens were dehydrated by steps in an ethanol series, and then cleared in methyl benzoate. Wholemount preparations remained in methyl benzoate for observation, photography, and permanent conservation. Some Paraplast-embedded pieces were sectioned parasagittally up to the

midline, and the remaining half (with a sharp midline) was deparaffinated and returned to methyl benzoate as a wholemount.

Given that the curvature of the neural tube halves impeded focusing them whole for microphotography with ×6.3 or ×4 microscope objectives, we positioned the specimens as desired on the concave slope of the Maximow slide concavity, submerged in methyl benzoate. This setup allowed taking “oblique” microphotographs focused selectively on the basal or alar aspects of the neural tube, or on any other portion of interest. In a few cases we resorted to the reconstruction of separately photographed focus planes.

The lizard *Lacerta gallotia galloti* eggs were collected with permission in the field in Tenerife (Canary Islands, Spain) during several yearly laying seasons. The eggs were incubated further at room temperature in the laboratory, enveloped in slightly humidified cotton in periodically ventilated containers. At appropriate intervals, the embryos were fixed and staged according to the developmental tables for *Lacerta vivipara* [Dufaure and Hubert, 1961] (abbreviated DH) and *Lacerta gallotia galloti* [Ramos, 1992]. This study comprises data sampled from practically all stages between stages 20 and 32. The rest of the procedure was like in chick embryos.

In the case of rat embryos, our AChE protocol consisted of overnight fixation in a cold phosphate-buffered paraformaldehyde solution, and subsequent wholemount incubation (usually overnight) at 4°C of the partly dissected and bisected embryo forebrains (cut at the isthmus) according to Karnovsky and Roots [1964]. We found that the rat embryonic AChE was more sensitive to paraformaldehyde than chicken AChE. We thus reduced the concentration of paraformaldehyde from 4% to 1%, and, after various empiric trials, selected a pH 5.7 Tris/maleate buffer solution in the incubation solution, instead of the original pH 6 acetate buffer used with chick embryos. The reaction was stopped by buffer washes after its progress was judged sufficient by visual inspection. The forebrains were then halved, and all tissues external to the neuroepithelium were peeled off manually under a magnifying microscope. The clean specimens were dehydrated in an ethanol series and cleared in methyl benzoate.

In some cases, we further dissected the specimens eliminating the telencephalic vesicle to facilitate flat mounting under a coverslip, which was elevated by pieces of coverslip under the corners. Some tears sometimes appeared at this point. Moreover, some resected specimens were embedded in paraffin and serial 10 μm-thick sections were obtained. The weak staining observed in this material was successfully intensified by overnight exposure of the slides (after deparaffination and hydration) to osmium tetroxide vapor in glass slide racks placed in a closed chamber holding a small amount of 1% OsO<sub>4</sub> solution at the bottom.

## Results

We will first reexamine the early forebrain data published in Puelles et al. [1987a] (stages 11–18, i.e., up to 2.5 days of incubation), profiting to correct some interpretive errors that we detected in retrospect. Then we proceed with our correlative unpublished chick AChE results for the period of 3–5 days of incubation [Amat, 1986]. Basal and alar plate data will be described separately. Note that

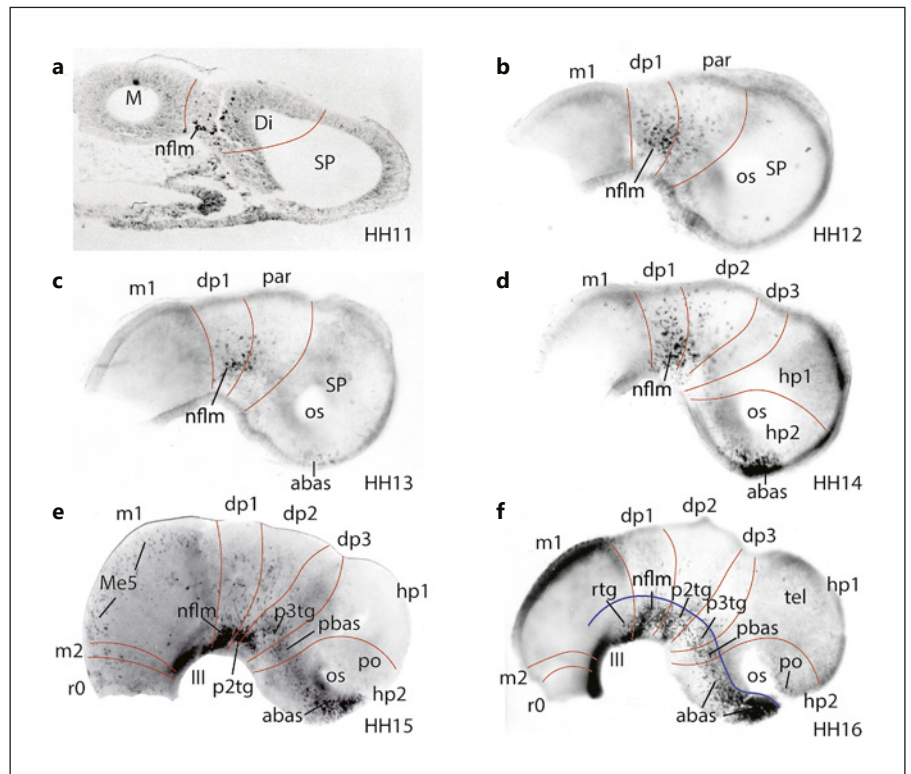


**Fig. 2.** Chick AChE-reacted material at stages HH11-HH16. Red lines separate anteroposterior partitions (proneuromeres or neuromeres). **a** Sagittal forebrain section at HH11 showing earliest postmitotic neurons of the nflm basal cell group at the caudal diencephalon (Di). M = midbrain; SP = secondary prosencephalon. **b** Wholemout at HH12. The diencephalon has produced already prosomere dp1, where most differentiated nflm neurons appear, while the larger rostral parencephalic region (par) is not yet divided into dp2 and dp3. **c** Wholemout at HH13, showing a second incipient basal cell group – abas – at the rostralmost (acroterminal) part of the secondary prosencephalon (SP), apart of increased nflm cells at basal dp1. **d** Wholemout at HH14. The abas cell group is now much more populated, and the remaining neuromeres have appeared (dp2, dp3 and hp1, hp2), so that it now clearly lies in hp2. Note hp1 contains dorsally the telencephalic primordium, while hp2 contains the eye vesicle (cut at the optic stalk, os). The m1 mesomere remains fully undifferentiated. There appear also some alar neurons in dp1 and dp2. **e** Wholemout at

HH15. Apart of the previous basal cell groups nflm and abas, additional basal groups have appeared: p2tg in dp2, p3tg in dp3, and pbas in hp1. Group abas has started to extend bilaterally caudward, under the optic stalks (forming the “abas wings”). There remains a gap between abas and pbas. At the basal m1 there appears the oculomotor nucleus (III). Incipient alar neuronal populations are observed in m1 (the Me5 dorsal cell group), dp1, and dp2. **f** Wholemout at HH16. All the forebrain neuromeres except the retarded m2 have developed basal plate cell groups. In m1, the rtg (rubral tegmental) group has emerged rostrally above the III. The other cell groups have established mutual contact, thus building jointly a basal plate band of neurons, which is still rather sparsely populated in some parts. A blue line was traced indicating the position of the alar-basal boundary. At HH16 the earliest neurons start to appear at the preoptic area (po) within hp2, just dorsal to the optic stalk (os). The epiphysis protrudes out at the center of the dp2 roof, and the telencephalic outpouching is visible.

each distinct emerging positive cell or cell group is heterochronic relative to surrounding elements appearing earlier or subsequently. Such heterochrony is best noticed initially, at the start of neurogenesis, since it tends to become less distinct as soon as the available space of each structural subunit becomes uniformly covered by neurons. We will next present one after another similar observations on the forebrain from the lizard and rat embryonic AChE material (the latter extracted from Puelles et

al. [2015b]). The last section illustrates heterochronic neurogenetic data on the chicken embryonic hindbrain (unpublished material from Amat [1986]), with a glance at selected rat hindbrain data.

### B – Chick Forebrain Patterns

#### B.1 – The Basal Forebrain Longitudinal Domain

The earliest forebrain AChE-positive neurons appear caudally at stage 11 in the diencephalic proneuromere

(site of prospective dp1 prosomere), roughly at dorsoventral mid-levels of the lateral neural wall (Fig. 2a; we refer to Hamburger and Hamilton [1951] stages). Subsequent development by stages 12–14 increases the number of postmitotic neurons at this dp1 site identified as nfm (nucleus of the medial longitudinal fascicle, a.k.a. interstitial nucleus of Cajal) (nfm; Fig. 2b–d). This patch remains well delimited rostrally and caudally. It soon becomes evident by disproportionate growth of the overlying undifferentiated alar plate that these earliest nfm neurons actually belong to the developing basal plate, which increasingly occupies a relatively more ventral locus (it is unclear whether some amount of dorsoventral displacement of the differentiating cells occurs). It is interpreted that the prospective forebrain alar plate is tiny in the early neural tube, and the prospective basal plate relatively larger, but the alar plate grows differentially due to its exponential mode of proliferation, whereas the basal domain does not expand so much (compare with the proportions at stage 16; Fig. 2f). Remarkably, the precociously differentiated population of the caudal diencephalic basal plate does not expand from this initial dp1 locus either rostralward, or caudalward into the midbrain. Neither midbrain or hypothalamus show any neurogenesis at stages 11 and 12 (Fig. 2a, b).

At stage 13 we first see a new AChE-positive cell group – abas – which emerges tenuously in the hypothalamic proneuromere (SP) at median acroterminal basal plate level of the prospective hp2 (i.e., far apart from nfm). Subsequently, at stage 14, this population appears better developed (abas; Fig. 2c, d). This cell patch was originally identified as “arch” (retrochiasmatic area) [Puelles et al., 1987a], but Puelles et al. [2012a] renamed it *anterobasal nucleus* or area (abas), following the apt term introduced by Altman and Bayer [1978, 1988]. The midbrain remains devoid of any neurogenesis at stages 13–14 (m1; Fig. 2c, d).

Nevertheless, a few isolated AChE-positive neurons can be distinguished at basal dp2 and dp3 diencephalic levels already at stage 14, which we now interpret as *p2 tegmentum* (p2tg) and *p3 tegmentum* (p2tg; p3tg; Fig. 2d; these substitute the vague or inaccurate older names “atp” – area of the tuberculum posterior – and “arm” – retromamillary area) [Puelles et al., 1987a]. All these basal sites appear more abundantly populated by stage 15. At stage 16 the dp2 cell group p2tg shows a prominent extension ventralwards (compare p2tg in Fig. 2e, f), and the group abas expands bilateral wings oriented caudalwards under the optic stalks, roughly up to the limit with hp1, which appears free of differentiation at stage 15, but shows earli-

est neurons of the prospective *posterobasal group* – pbas – at stage 16 (abas; pbas; Fig. 2e, f). The pbas notion also derives from Puelles et al. [2012a]; it had been misinterpreted as “amaml” (lateral mamillary area) in Puelles et al. [1987a].

Moreover, at stage 15 the first ventral basal cell group appears in the m1 midbrain unit, which we identify as the anlage of the oculomotor nucleus (3); it appears more distinctly developed at stage 16 (3; Fig. 2e, f). We also observed at stage 16 another incipient postmitotic population at the rostral end of midbrain basal m1, not well delimited from nfm, and located just above the 3. This forms an incipient population that we now identify more precisely as the rubral tegmental area or rtg (rtg; Fig. 2f); previously we called it imprecisely “ateg,” or “tegmental area”). Note that all early neuromeric basal populations identified so far in the midbrain, diencephalon, and hypothalamus will later occupy a dorsal part of the adult basal plate, whereas the corresponding void ventral or paramedian basal domains of early embryos will become populated subsequently, often producing different basal neuronal types (e.g., mesodiencephalic dopaminergic neurons – an evidence of forebrain tagmatic mesodiencephalic similarity, or hypothalamic tuberal and mamillary neurons – hp2 –, and retrotuberal and retromamillary neurons – hp1). It thus seems that the modular basal plate domain is heterochronic and uniformly *starts to develop at its dorsal border* with the alar plate and thereafter expands ventralwards towards the underlying paramedian basal subdomain that shows relatively retarded neurogenesis next to the floor plate.

During the following stages 17–19 the different basal cell groups (abas, pbas, p3tg, p2tg, nfm, 3, and rtg) previously emerged in a disjoint order along hp2, hp1, dp1, dp2, dp3, and m1 cohere gradually by further intercalated addition of neurons forming an apparently continuous columnar arrangement known as the *basal plate band* (Fig. 3a–c). Note this band is not continuous caudally with the hindbrain, due to the largely undifferentiated m2 neuromeric unit. This is part of the evidence (apart from various shared vs. differential molecular patterns) indicating that the midbrain belongs developmentally to the forebrain tagma, contrary to the classic neuroanatomic notion that it is a separate vesicle intercalated between forebrain and hindbrain. In contrast with the much retarded caudal midbrain unit (m2), the rostral hindbrain progresses separately in its neurogenetic program (in our forebrain specimens we occasionally see attached to the caudal midbrain the AChE-positive anlage of the isthmic trochlear motor nucleus (4) (e.g., Fig. 3c). At stages 17–20

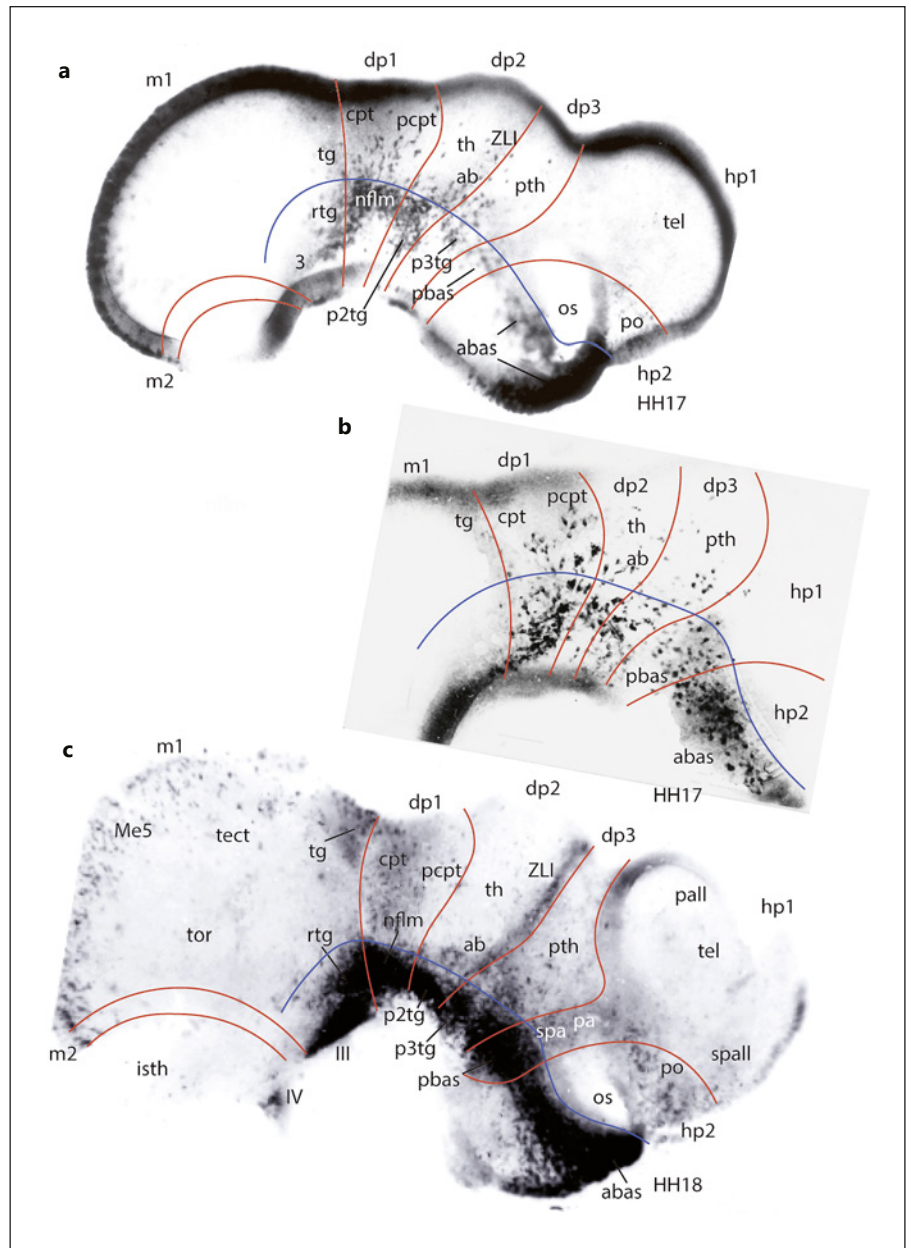


**Fig. 3.** AChE-reacted chick forebrain wholemounts at HH17 (**a, b**) and 18 (**c**). Red lines separate anteroposterior partitions (neuromeres). A blue line enclosing the basal plate band separates basal plate from alar plate. **a, b** These specimens were oriented for preferential focus on the basal plate. Some basal cell groups extend ventralwards towards the floor plate across the interposed undifferentiated *paramedian basal domain* (e.g., p2tg and p3tg). The alar pretectal cells in dp1 appear subdivided into the molecularly distinct commissural and precommissural pretectal areas (cpt; pcpt). Thalamic alar cells largely concentrate at the incipient anterobasal area (ab), which contacts both the basal plate and the emergent and increasingly AChE-positive zona limitans intrathalamica separating th/dp2 from pth/dp3 (ZLI; not seen in **b**). There is also a small group of prethalamic alar neurons. **c** At stage HH18 the basal plate band is much more compact, though the individual neuromeric

modules are still partially identifiable. The alar midbrain shows a well-developed dorsal Me5 population, but the tectal domain is still essentially undeveloped. Only rostrally, behind the pretectum, a rostral m1 alar domain starts to develop, identified as the tectal grey area (tg). The pretectal cpt subarea is more populated than its pcpt counterpart (alar dp1). At the thalamus (th; alar dp2) we still see only the ab cell group. The ZLI shows strong neuroepithelial AChE activity. At the prethalamus (alar dp3) most alar neurons concentrate in a posterobasal area in front of the ZLI (pb). The alar part of hp1, found behind the optic stalk, shows the earliest paraventricular and subparaventricular cell groups (pa; spa), which later will expand rostrally into alar hp2, dorsally to abas. The pre-optic area shows at this stage a distinct neuronal population (po). The telencephalon remains wholly undifferentiated.

the initially unpopulated ventral or paramedian parts of the different neuromeric basal plate areas increasingly display clear-cut ventralward extension of the basal populations, particularly at the hypothalamic hp2 abas unit (Fig. 3a–c, 4a, b).

At stages 19 and 20 the basal plate band of AChE-positive neurons is thicker and better developed, though the individual neuromeric basal plate components can still be roughly identified, particularly abas, pbas, p3tg, p2tg, and nfm, due to their advancing front at the ventral border of the basal band, where each of these populations extends ventralward separately with an irregular spike of cells (Fig. 4a, b). Remarkably, the basal plate of m2 still remains devoid of neurons, appearing as a neuron-less unstained domain intercalated between the 3 in m1 and the 4 within the isthmus (Fig. 4a, b). At stage 22 the growing rtg midbrain cell group shows a gradential distribution of its population, decreasing caudalwards in its cellular density (rtg; Fig. 5a).

At stages 24 and 26 the basal plate band has developed further but is now too thick to admit efficient penetration of the histochemical reactives, so that we lack an accurate AChE image (Fig. 6a, b).

## B.2 – The Alar Forebrain Longitudinal Domain

The earliest alar postmitotic neurons of the forebrain tagma that develop AChE reaction were seen at stage 13 in the midbrain (Fig. 2c) [see also Puelles et al., 1987a; their Fig. 5a, b]. These alar cells surprisingly lie along the midbrain roof plate and adjacent dorsalmost alar plate. They represent the singular Me5 population (mesencephalic trigeminal nucleus), which appears simultaneously along both m1 and m2. There is a sharp caudal limit of Me5 at the isthmo-preisthmic (r0/m2) boundary. These neurons later have typological, hodological, and molecular features of sensory ganglion neurons, which normally derive from neural crest or placodal sources. There is a theory that neurulation occurs at midbrain levels so rapidly that part of the neural crest material does not separate from the alar and roof plates and remains locked inside the midbrain after the closure of the roof. The derived sensory ganglion cells thus differentiate at the dorsal locus where one would expect to see any neural crest remnants, that is, close to the roof plate. In some chicken breeds, other neural crest derivatives such as melanocytes are found mixed with the Me5 population [Puelles and Gil, 1978]. In a way, therefore, considered as an hypothetical ectopic neural crest derivative Me5 does not truly belong to the midbrain alar plate.

Properly alar neurons are first seen dispersed at pre-tectal (dp1) level at stage 14, and they grow in number at stages 15–16, becoming very obvious at stage 17, divided into commissural and precommissural pre-tectal micro-zones (cpt; pcpt; Fig. 2d–f, 3a, b). At stage 17, the thalamic alar domain (dp2) has only very few differentiated neurons, mainly found ventrally in an area known as “antero-basal progenitor area” (ab), next to the incipient zona limitans intrathalamica, a glial palisade with secondary organizer functions (ab; ZLI; Fig. 3a, b) [Martínez-de-la-Torre et al., 2002]. Alar cells also start to emerge in the alar prethalamus (dp3), also mainly ventrally (pth; Fig. 3a, b); this precocious microzone corresponds to the prospective prethalamal *zona incerta* [Puelles et al., 2012a, 2021].

The rostralmost part of the alar optic lobe starts to show AChE-positive cells of the prospective *tectal gray* retinorecipient center [García-Calero et al., 2002; Puelles, 2019; Puelles, 2022] at stages 17–18 (tg; Fig. 3a–c). The precocious midbrain tg is next followed caudalwards by the more retarded optic tectum and auditory torus semi-circularis microzones, both sparsely populated over stages 19–20 (tect; tor; Fig. 4a, b) [Puelles et al., 1994, 2019a].

At stage 19 there appears a well-delimited emergent neuronal group occupying selectively an intermediate dorsoventral sector of the dp2 thalamic alar domain (th; Fig. 4a), probably corresponding to an early born superficial thalamic nucleus, the superficial magnocellular nucleus of Rendahl [1924], studied in Puelles et al. [1991] and Martínez et al. [1991]. The primordium of the epiphysis at the dp2 roof also starts to show AChE activity at stage 19, though it is devoid of neurons (ep; Fig. 4a, b). We also found from stage 18 onwards the earliest hp1 and hp2 hypothalamic alar neurons outside the eye and telencephalon, namely at the regions later occupied by the sub-paraventricular and paraventricular areas, which later expand into hp2 over and under the optic stalk (spa; pa; Fig. 3c, 4a, b) [Puelles et al., 2012a]. Earliest neural retina ganglion cells differentiate from stage 15 onwards [Prada et al., 1981; Puelles, 2009; L.P., unpublished AChE data]; the whole eye evaginates early on out of an acroterminal alar hp2 subarea lying under the prospective preoptic area; this is represented in our material by the cut optic stalk (os). Other secondary prosencephalic alar neurons emerge gradually at the preoptic area (telencephalic alar subdomain of hp2) during stages 17–20 (po; Fig. 3a, c, 4a, b).

The alar populations advance significantly in cell numbers at stages 19 and 20. Remarkably, the preisthmic m2 domain continues undifferentiated, excepting its partici-

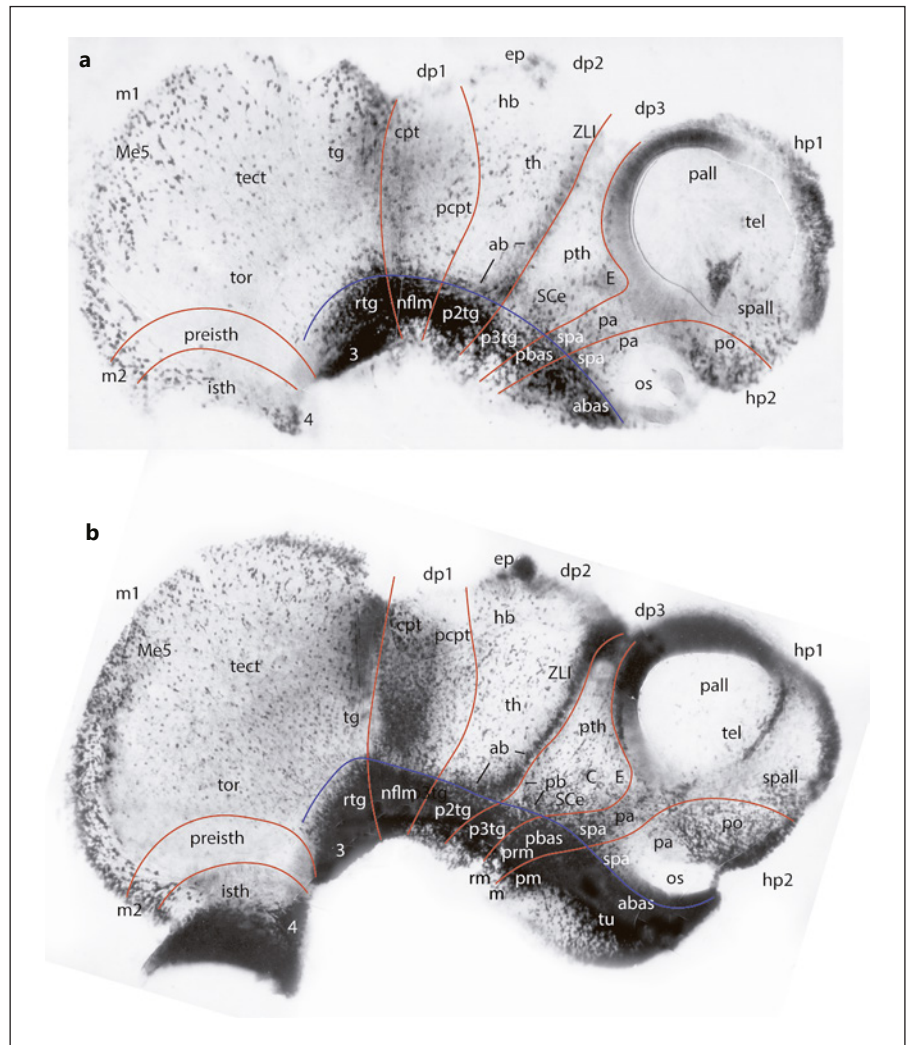


**Fig. 4.** AChE-reacted chick forebrain wholemounts at HH19 (**a**) and HH20 (**b**). The basal plate band continues to consolidate at these stages, with added expansion ventralwards into the retarded paramedian basal territory. **a** At stage 19 there appear dispersed pioneering neurons in the m1 tectal area (tect), caudally to the more precocious tectal grey area (tg). Caudally the prospective torus area remains unpopulated, as occurs with the preisthmic area in m2 (tor; preisth). The alar dp1 (pretectum) shows no significant change, whereas the alar dp2 (thalamus) displays at mid-dorsoventral level the first neurons of the principal thalamic area (th), caudal and above the ab cell group. A few neurons appear at the habenular thalamic area (hb). The epiphysis (ep) starts to show some neuroepithelial AChE reaction. The alar dp3 (prethalamus) has developed a distinct population ventrally, corresponding to the future “subcentral” incertal area (SCe), as well as early neurons at the future “eminential” area (E). In the alar hypothalamus the pa and spa areas start to expand into hp2. The telencephalic subpallium

(spall; hp1) starts to have postmitotic neurons, whereas the preoptic area (po; hp2) increases its population. **b** At stage 20 the hypothalamic basal plate shows novel paramedian differentiated areas identified as periretromamillary (prm) and perimamillary (pm) in hp1 and hp2, respectively; these lie just over the still undifferentiated sites of the prospective retromamillary and mamillary areas (rm; m). The alar m1 domain expands distinct tg and tect populations and shows now also some toral area cells (tor). The Me5 population is still distinct dorsally and clearly reaches also the m2 unit. There appears some neuroepithelial background AChE activity at the rtg (m1) and the cpt (dp1). The epiphysis (ep; dp2) shows strong neuroepithelial AChE activity, and so does the dorsal end of the ZLI (compare with **a**). The alar hypothalamic spa and pa areas (hp1, hp2) as well as the telencephalic spall and po areas (hp1, hp2) are more developed. The pa area in hp1 typically extends also dorsally into the telencephalic stalk, caudally to the spall (future hypothalamo-amygdalar corridor).

pation in the dorsal Me5 singularity (Fig. 4a, b). The tect and tor m1 alar subregions lying caudal to the precocious tg microzone now show likewise a dispersed population of neurons, slightly more numerous ventrally than dorsally; a rostrocaudal gradient is not observed (tect; tor; Fig. 4a, b). These are possibly just the earliest-born tectal neurons previously identified autoradiographically and histochemically as “solitary magnocellular neurons” of the tectal stratum griseum centrale [Martínez-de-la-Torre et al., 1987].

In the diencephalon, the alar pretectum (dp1) shows a caudal commissural pretectal domain (where the fibers of the posterior commissure course into the basal plate), which is most populated, as well as a rostral less populated precommissural pretectal domain that pushes the pretecto-thalamic boundary slightly rostralwards (Fig. 4a, b). We have shown that the pretectal alar domain is actually divided molecularly in anteroposterior direction into *three* progenitor areas named commissural, juxtacommissural, and precommissural areas, each producing a number of specific pretectal nuclei [Ferran et al., 2007, 2008, 2009]. It is possible that the incipient slender intermediate juxtacommissural area cannot be distinguished at these stages from the denser commissural area (cpt; pcpt; Fig. 4a, b).

The alar thalamus (dp2) shows at stage 22 a higher number of AChE-positive neurons, including some at the dorsocaudal habenular subdomain (ab; th; hb; Fig. 5a, b). The precocious boomerang-like anterobasal area – ab – next to the ZLI, extends also along the alar-basal border [see Martínez-de-la-Torre et al., 2002]. It continues to be the most populated thalamic area, followed by the dorso-caudal th area (with a gradient in dorsoventral direction). We have reported about a thalamic model in which three dorsoventral tiers (dorsal, intermediate, and ventral) are distinguished as thalamic pronuclei (primordia of various definitive thalamic nuclei), apart from the overlying, slightly caudal habenular area lying next to the thalamic neural roofplate (the latter is represented by the epiphysis – ep –, its stalk, and the chorioidal roofplate). The dorsoventral differences in the neuronal densities observed within the thalamic alar area at stages 20–22 suggest the postulated tier structure [Díaz et al., 1994; Yoon et al., 2000; Redies et al., 2000; Dávila et al., 2000; Puelles, 2001; Martínez-de-la-Torre et al., 2002; González et al., 2002].

The prethalamic domain (dp3) also shows at stage 22 an extensive alar population stretching with a subtle cell density gradient into the roofplate (pth; Fig. 5a, b). We recently examined prethalamic genoarchitectonic subdivisions [Puelles et al., 2021]. Dorsoventrally we identified

three parts: prethalamic eminence (E), central prethalamus (C), and subcentral prethalamus (SC), the latter corresponding to the classic zona incerta. Apart the unitary dorsal prethalamic eminence (which reaches the insertion of the roof chorioidal tela – ch), the central and subcentral domains are divided each in three distinct anteroposterior portions. There also exists a prethalamic mirror image of the thalamic anterobasal area (but placed rostrally to the ZLI) which we accordingly identified here as *posterobasal area* (pb; Fig. 5a, b).

As regards the alar hypothalamus, at stages 20–22 the alar populations spa and pa of hp1 appear well delimited from the neighboring alar prethalamic area (dp3) and the less populated alar terminal hypothalamus (hp2). The latter was partly lost during the dissection of the optic vesicle, which derives from its acroterminal subregion (PHyA; THyA; Fig. 5b). The previously described precocious telencephalic preoptic area seems now accompanied by parts of the hemispheric subpallium at stages 20–22 (po; spall; Fig. 4b, 5a). We distinguish in principle preoptic, diagonal, pallidal, and striatal subdivisions of the subpallium, all of which converge dorsalward upon the subpallial septum [Puelles et al., 2000; Bardet et al., 2010; Puelles et al., 2013]. Results at stages 20–22 suggest that postmitotic neurons have appeared at least at preoptic and diagonal subregions, and perhaps are incipient at the pallidal subregion, but are still absent from the more retarded striatum.

At stages 24 and 26 (4 and 5 days of incubation) the diencephalic alar plate shows a well-developed mantle layer at pretectal (dp1), thalamic (dp2), and prethalamic (dp3) levels (Fig. 6a, b). The pretectum is neatly limited dorsally from the more dorsally prominent habenular area of the thalamus. The pretectal boundary with the underlying tiered egg-shaped main part of the thalamus (dark th area in Fig. 6a at stage 24) is unclear in the stage 26 whole mount (Fig. 6b). The prethalamus is separated from the thalamus by the cell-poor ZLI boundary, best visualized at stage 26 (ZLI; Fig. 6b). The wholemount shows at the top of the populated parts of thalamus and prethalamus a transparent membrane, which is the diencephalic roof chorioidal tela, which is inserted caudally in front of the prospective habenular commissure (apparently not yet formed at these stages) which lies in front of the epiphyseal stalk (not seen).

Finally, the stage 26 wholemount also shows distinctly the superficial anterobasal area population – ab – that borders both the ZLI and the underlying basal plate, in a boomerang shape (ab; Fig. 6a, b).

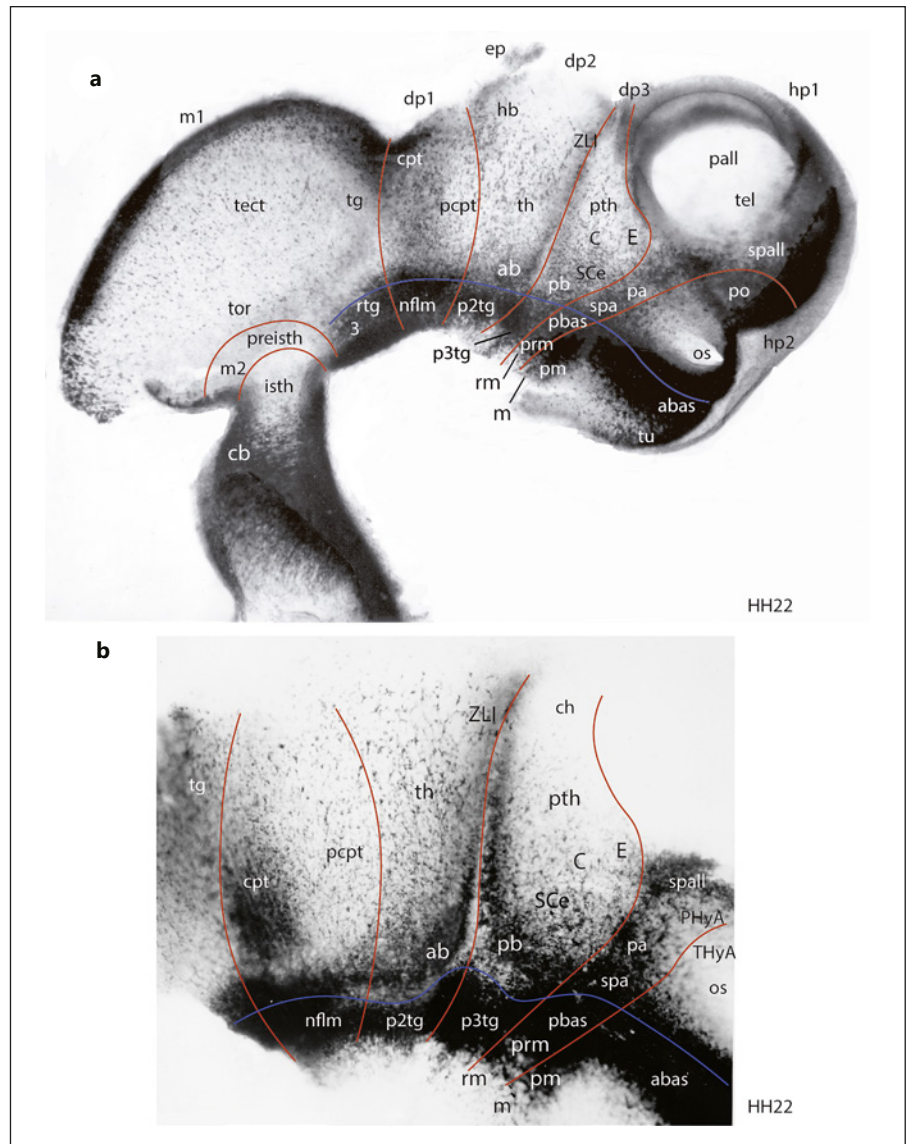


**Fig. 5.** AChE-reacted chick forebrain whole-mounts at HH22 (**a**, **b**). **a** An overview shows advanced alar development, particularly in the pretectum (cpt, pcpt; dp1), thalamus and habenula (ab, th, hb; dp2), and prethalamus (pb, SC, C, E; dp3), as well as in the alar hypothalamus and the subpallial and preoptic telencephalon (spall, po; hp1, hp2). **b** Higher magnification detail showing in particular the thalamic ab area and the prethalamic pb area, both of which relate intimately to the ZLI secondary organizer, whose (*Shh*-positive) core is marked by the red line (compare Fig. 15a).

### C – Lizard Forebrain Patterns

We next illustrate selected embryonic specimens from *Lacerta gallotia galloti* between stages DH25 and DH30 (Fig. 7), emphasizing similarities and differences with regard to chicken material. One peculiarity of the lizard embryos is that some forebrain neuroepithelial sites that showed marked AChE reaction in the chick (e.g., the zona limitans intrathalamica or ZLI, or the pretectal commissural area or cpt) did not do so in the lizard, whereas other neuroepithelial sites such as the isthmus organizer (IO; Fig. 7a, b, f) and the anterobasal hypothalamic region within THy (abas; Fig. 7a–g) showed a significant neuroepithelial reaction (in the latter case possibly coinciding

with local differentiating neurons mixed with the ventricular cells, rather than in a mantle layer, at least initially).

#### C.1 – Basal Plate

At stage DH25/25+, AChE-positive cells are already present along the basal plate modules of m1, dp1–dp3, hp1 and hp2 (rtg, n flm, p2tg, p3tg, pbas, abas), though the dp3 and hp1 components (p3tg, pbas) are still very weakly populated (Fig. 7a, b). The m2 remains unpopulated, as we saw in the chick. The oculomotor nucleus is clearly observable within basal m1 at stages DH26/26+ (3; Fig. 7c, d). The initially retarded basal parts are more advanced at

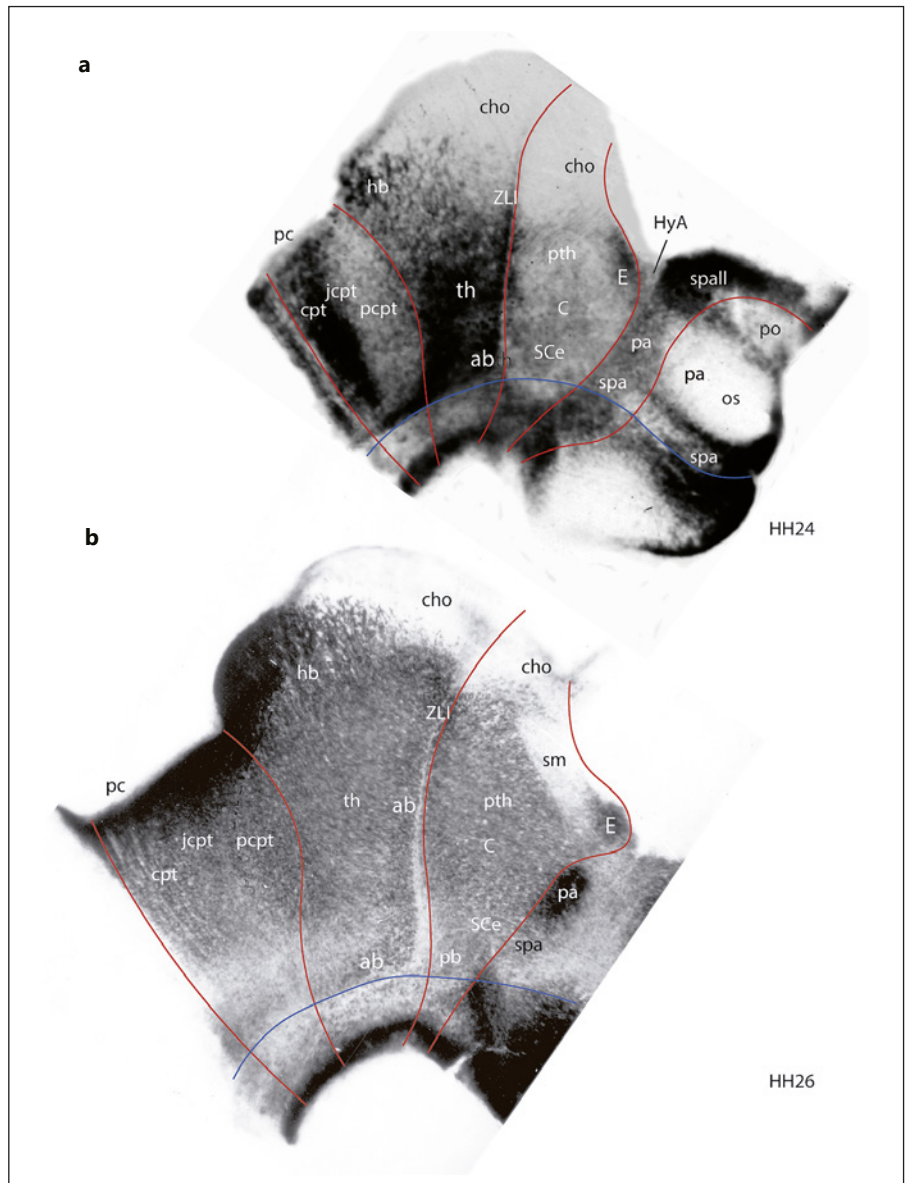
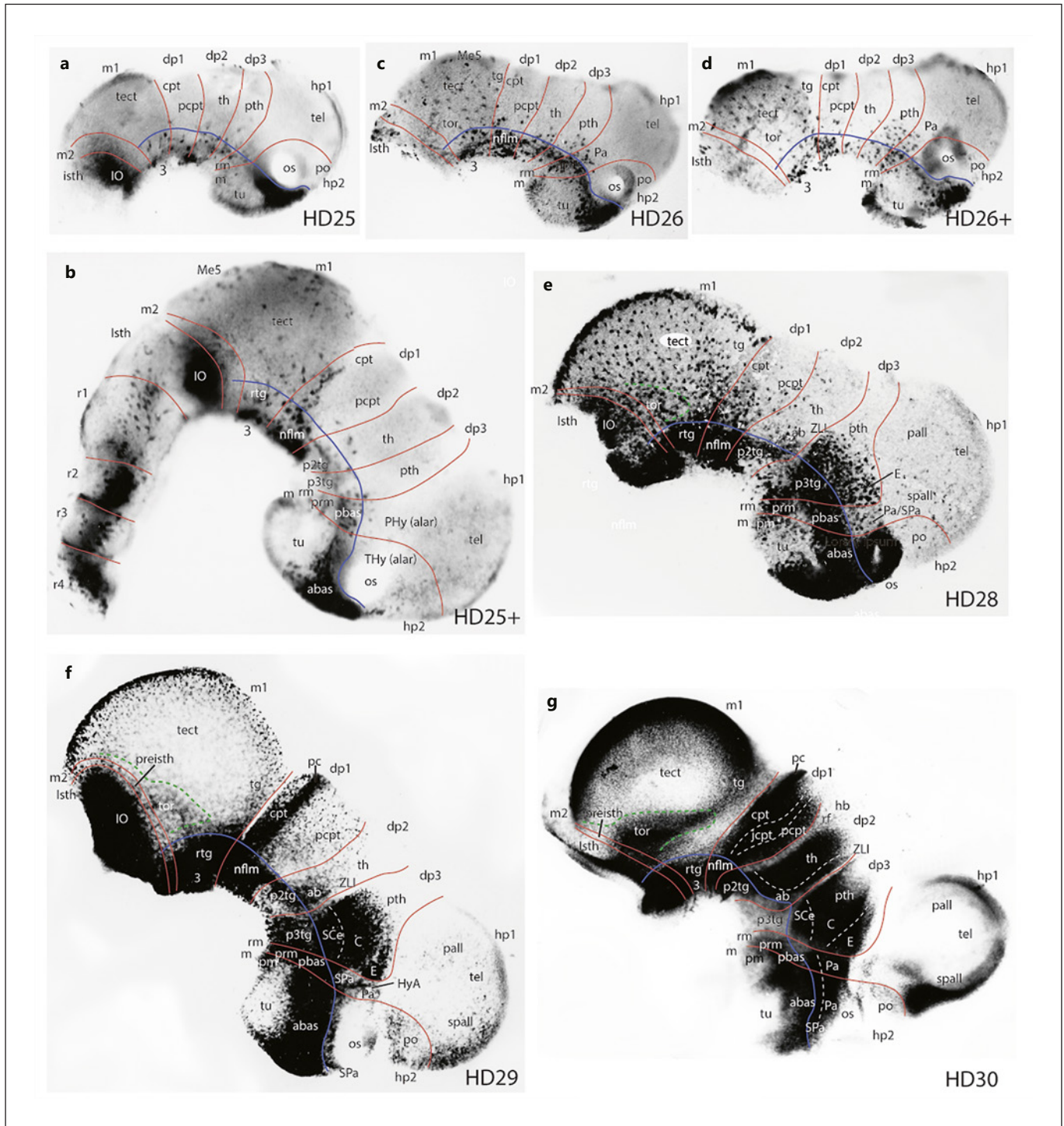


**Fig. 6.** AChE-reacted chick forebrain wholemounts at HH24 (**a**) and HH26 (**b**). These images show mainly the alar diencephalon, distinctly oversized now compared with the underlying basal plate (blue line). **a** At stage 24 (4 days of incubation) the pretectum (alar dp1) starts to show its underlying molecular division into the commissural, juxtacommissural, and precommissural domains (cpt, jcpt, pcpt). The thalamus (alar dp2) displays a massive central ovoid mass (th) above the ab area (indistinct here), and a clear-cut habenular area (hb), not yet fully expanded dorsalward. The prethalamus (alar dp3) is now uniformly covered by neurons (SCE, C), which show low AChE activity (similarly as the pcpt population), except the molecularly distinct eminential subpopulation limiting caudally the interventricular foramen, which displays higher AChE (E). Both thalamus and prethalamus show their AChE-negative chorioidal roofplate which starts in front of the epiphysis (the habenular commissure is not formed yet). The alar hypothalamic pa and spa areas (a.k.a. “supraopto-paraventricular

area”) are also well developed across hp1 and hp2, and the dorsal spike of the pa area clearly enters dorsalward the floor of the interventricular foramen, forming the hypothalamo-amygdalar corridor (HyA). **b** At stage 26 (5 days of incubation), the alar diencephalon appears uniformly covered by neurons, except at the ZLI cell-poor central gap (representing a radial glia palisade). The cpt, jcpt, and pcpt subdomains of the pretectum are distinguishable (note the fibers of the posterior commissure – pc – running ventralwards strictly along cpt). The thalamic ab, th, and hb subdomains are also distinct (note a dorsalward expansion of hb when compared to that in **a**). The different prethalamic domains (pb, SCE, C, E) also have reached their full areal extent, particularly by dorsal expansion of both C and E (the stria medullaris tract courses longitudinally through E, ZLI, and hb towards the habenular commissure that forms behind the caudal end of the diencephalic chorioidal roofplate).

stage DH25+, at which a complete but not yet compact basal plate band is visible, further amplified at stage DH26 (Fig. 7b, c). The paramedian tuberal hypothalamic area remains largely undifferentiated at these stages (tu; Fig. 7a–d). Basal plate compaction advances notably at

subsequent stages (Fig. 7c–f), though there remains a noticeable gap at the level of the incipient zona limitans cell-poor transversal core (dp2/dp3 limit) as of stage DH28 (ZLI; Fig. 7e–g; note lack of neuroepithelial AChE at the ZLI); this gap was not seen in the chick. Likewise, the peri-



(For legend see next page.)

retromamillary and perimamillary ventrobasal hypothalamic areas next to the retarded retromamillary and mamillary areas of hp1 and hp2 start to be populated as of stage DH28, while the tuberal area remains retarded in this aspect (prm, pm; Fig. 7e, f). Midbrain and diencephalic basal areas also expand into the retarded paramedian domain (Fig. 7e, f). At stage DH30 the thickness of the basal plate starts to hinder efficient penetration of histochemical reactives, so that less detail could be observed basally (Fig. 7g).

### C.2 – Alar Plate

As regards the reptilian forebrain alar plate, the dorsal Me5 population first appeared at stage DH25+, accompanied already by sparse tectal AChE-positive cells (Me5; tect; Fig. 7b). The latter increase in number at stages DH26, 26+, and 28 (tect; Fig. 7c–e). Though they initially are distributed rather homogeneously within alar m1, starting at stage DH28 into DH30 two subareas with increased cell density are observed, thought to correspond to the incipient rostrally placed “tectal grey domain” (tg;

Fig. 7e–g), and the caudoventrally placed “torus semicircularis”; we surrounded the latter by a dashed green limit (tor; Fig. 7e–g; the torus is the sauropsidian homolog of the mammalian inferior colliculus). The m2 alar plate (or preisthmus) remains largely undifferentiated up to stage DH26+ but shows an incipient population at stages DH28–30 (preisth; Fig. 7e–g). The midbrain alar plate thus seems to progress in neurogenesis relatively earlier than the diencephalic counterpart, which contrasts with the opposite pattern in chicken.

The diencephalic alar plate seems largely undifferentiated at stage DH25 (Fig. 7a), but shows a group of caudal cells at stage DH25+; these cells correspond to the *commissural* pretectum (alar dp1), since they coincide with the caudal locus where the fibers of the posterior commissure are going to course subsequently (cpt; Fig. 7b). This population is not more developed in our stage DH26/26+ specimens (Fig. 7c, d), but is clearly more abundant at stage DH28 (cpt; Fig. 7e), and is now accompanied by additional cells in the *precommissural* pretectum domain (pcpt; Fig. 7e). At stages DH29/30 the pretectum shows

**Fig. 7.** AChE-reacted wholemount forebrain preparates of lizard embryos at different stages (a–g). The interneuromeric boundaries are traced in red, while the alar-basal boundary is represented by a blue line. Note that, in contrast to chick embryos, lizard embryos show strong neuroepithelial AChE activity at the locus of the isthmic organizer (IO; a site where FGF8 is released), but do not show neuroepithelial AChE signal at the diencephalic ZLI (a site where SHH is released; compare Fig. 15b). **a** At stage HD25 most basal plate areas are partly populated (rtg, nfm, p2tg, p3tg, abas), but pbas still shows sparse neurons. There is no alar differentiation. **b** At stage HD25+ the forebrain basal plate modules are all visible, and alar differentiation has started at the m1 tect and Me5 areas, as well as at the cpt area (alar dp1) and the thalamic incipient ab area (dp2). See also wholemount AChE staining at pontine and prepontine parts of the hindbrain down to r4 in **b**. **c, d** Between stages HD26 and 26+ the AChE image hardly changes. Within m1, additional dispersed cells appear at the tect and Me5 areas, whereas the neighboring tg or tor areas are retarded or undistinct. Within the alar diencephalon, the prethalamic component (pth) is most advanced. The first positive cells emerge at the alar hypothalamic Pa area. The preoptic area (po) remains unpopulated. **e** The stage HD28 specimen shows considerable progress in its alar cell groups. The midbrain m1 and m2 units both show abundant AChE-positive cells. Earliest tg and tor cells have been added to the pre-existent tect and Me5 ones. The tor has a peculiar shape, here traced by a green dash line. The pretectum (alar dp1) shows more cpt cells, and less numerous pcpt cells. The thalamus (alar dp2) has a better developed ab cell group and some dispersed th cells dorsal to it. The prethalamus (alar dp3) is still the most developed subregion (pth), showing abundant positive cells in a ventrodorsal gradient, well delimited from the neighboring units. Its dorsalmost cells next to the telencephalic part of hp1 probably represents the

anlage of the prethalamic eminence (E), whereas the rest must contain the prospective central and subcentral prethalamus subdomains (compare **g**). The alar hypothalamic areas Pa/SPa are retarded with respect to the alar prethalamus. Sparse preoptic neurons are present (po; this contrasts with precocious local neurogenesis in the chick), as well as sparse subpallial telencephalic cells (spall). **f** At stage HD29, the m2 midbrain unit shows a distinct preisthmial alar population (preisth), just behind the m1 torus (tor; traced with a green dash line). The pretectal cpt domain shows AChE-positive fibers of the posterior commissure (pc). The thalamic ab area is now much better developed and notably ascends behind the ZLI. There are otherwise still very few central thalamic cells (th), and no habenular differentiation. The prethalamus (alar dp3) can now be subdivided into its subcentral (SCE; prospective incertal), central (C), and eminential (E) portions; the latter appears well delimited from the rest and starts to bulge behind the prospective interventricular foramen. The alar hypothalamic areas SPa and Pa which first emerged in alar hp1 are distinct and have expanded rostrally into hp2. The hp1 Pa component has expanded into the floor of the interventricular foramen, forming the hypothalamo-amygdalar corridor (HyA). Preoptic area and subpallium are better populated (spall, po). **g** At stage HD30 the forebrain alar plate is fully covered by neurons, excepting the cell-poor gap of the ZLI and pallial parts of the telencephalon. In m1 the torus (tor; green dash limit) has elongated, theoretically by addition of more caudal elements next to the preisthmus. The three anteroposterior subdomains of the pretectum were delimited by white dash lines (cpt, jcpt, pcpt), similarly as the main dorsoventral parts of the prethalamus (SCE, C, E). In the hypothalamus, the SPa alar area extends rostrally intercalated between the abas area and the rostral part of the pa area on top of the optic stalk.

higher cellularity, always with predominance of cpt over pcpt, and the cpt area appears covered by AChE-positive fibers of the posterior commissure (cpt; pcpt; pc; Fig. 7f, g). We indicated by dashed white lines the approximate location of the initially less distinct intermediate *juxta-commissural* pretectal domain, as identified in the adult lizard (jcpt; Fig. 7g) [Martínez-de-la-Torre, 1985; Medina et al., 1992, 1993; see also Ferran et al., 2007, 2008 for chick and mouse].

The thalamic alar plate (dp2) is slow in starting neurogenesis (Fig. 7a–d). At stages DH28/29 we see a distinct differentiating *rostroventral* cell group, probably the primordium of the *anterobasal* thalamic subdomain (ab; Fig. 7e, f). This enlarges subsequently both caudalward (ventrally) and dorsalward (rostrally, behind the ZLI; ab; Fig. 7g). In Figure 7g we separated with a dashed white line this subdomain from the rest of the thalamus (the larger caudodorsal – cd – histogenetic subdomain, site of th); at this stage the AChE-negative retroflex tract (rf) courses dorsoventrally just in front of the dp1/dp2 boundary (coinciding with a limiting cell-poor cleft; this indicates that the habenular dorsal subregion of th also must be differentiating, though we do not distinguish it in these preparations, either due to its artefactual loss, or because its neurons do not express AChE (ab; th; hb; rf; Fig. 7g).

The prethalamic alar plate (dp3) is more progressive than the thalamic counterpart in the lizard embryos, in contrast with the contrary pattern in the chick (but is still in retard relative to the midbrain m1 alar domain). Indeed, pth appears non-populated even at stage DH25+ (Fig. 7a, b). At stages DH26/26+ a distinct alar prethalamic cell group first emerges, accompanied by neighboring *paraventricular/subparaventricular* cells in the alar peduncular hypothalamus, or hp1 (pth; Pa; Fig. 7c, d). At stage DH28 the pth mantle is much more developed and pushes dorsalward into the telencephalon, starting to build the posterior limit of the incipient interventricular foramen with its eminential subregion (see below); the neighboring paraventricular cells show less massive development (pth; Pa; Fig. 7e).

At stages DH29/30 we see continued massive growth of the prethalamic mantle zone (much more advanced than the thalamic one). At stage DH29 we first distinguish what is going to be the *prethalamic eminence* (E; Fig. 7f), which was classically misidentified as “thalamic eminence.” This slightly separate *eminential* cell group relative to the rest of pth owes its name to the bulge it makes later at the posterior aspect of the interventricular foramen. It extends into the prethalamic part of the chorioidal roof (not shown) [see Puelles, 2019]. The main part of pth

found under the E is known to be subdivided dorsoventrally into central (C) and subcentral (SCe) histogenetic portions in the mouse [Puelles et al., 2021], but such parts cannot be distinguished yet in this material. These three E, C, SCe prethalamic subdomains are delimited by dashed white lines in Figure 7f, g. The SCe area produces the adult zona incerta, while the C area produces the pregeniculate, subgeniculate, and reticular nuclei, apart from other minor derivatives (see molecular delimitations in Puelles et al. [2021]).

Finally, as regards the hypothalamic alar plate (hp1, hp2), it appears wholly undifferentiated at stage DH25+ (Fig. 7a, b). The earliest cells appear at stages 26/26+ at the paraventricular/subparaventricular domain of hp1 (Pa), just in front of the pth and caudal to the optic stalk (Pa; os; Fig. 7c, d). The Pa region appears increasingly populated at stages DH28/20 (Pa; Fig. 7e, f); the *subparaventricular alar hypothalamic area* can be distinguished specifically at stage DH29 as a longitudinal alar population immediately dorsal to the alar-basal boundary, both through hp1 and hp2, as it was first defined (SPa; Fig. 7f) [Puelles et al., 2012a]. The parallel rostral extension of the overlying *paraventricular alar hypothalamic area* (Pa) into hp2 or THy is more difficult to see because it advances into the optic stalk (supraoptic area), and this was cut in our specimens when the eyes were dissected away. We thus estimate that this area probably already extends into the stalk at stage DH29. The full extent of both differentiated Pa and SPa areas was apparent at stage DH30, where we indicated their mutual longitudinal boundary with a dashed white line (Pa; SPa; Fig. 7g). Note Pa relates caudally with E, whereas SPa relates to C/SCe.

The telencephalic field represents the *dorsalmost* alar subdomain of the secondary prosencephalon (i.e., dorsal to the alar hypothalamus; see alar PHy and THy in Fig. 7b). It is represented as a vesicular evagination within hp1 and as the non-evaginated preoptic region within hp2 (tel; po; Fig. 7a–g). The preoptic area obviously is topologically dorsal to the optic stalk and the related eye vesicle. In contrast with the precocious neurogenesis observed in the chicken po, in the lizard this hp2 area, as well as the tel vesicle in hp1, remain unpopulated up to stage HD26+ (po; tel; Fig. 7a–d). At stage DH28 we observed the earliest differentiating cells in the subpallial area of the telencephalon, jointly with fewer cells in the preoptic area (tel; spall; po; Fig. 7e). Both populations are increased significantly at stage DH29 (spall; po; Fig. 7f).

## D – Rat Forebrain Results

Given that our rat data were reported before in some detail, including sectioned specimens [Puelles et al., 2015a], we will just compare their general aspects with the sauropsidian material, and eventually correct or add some interpretive details. We show early rat forebrain AChE patterns at E11 and E11.5 in Figure 8a–e; Figure 8b is a flattened wholemount at E11, and Figure 8f is a graphic reconstruction of the neuromeric ventricular relief at E11.5 (obtained from a series of semithin sagittal sections). Figure 9a–c shows flattened wholemounts at E12, E13.5 and E14.5.

### D.1 – Basal Plate

Emergence of AChE-positive cells in the E11/11.5 rat embryos resembles chicken stages HH13/14, insofar as the basal plate band is barely sketched but not fully developed yet. The hypothalamic hp2 anterobasal cell group (tagged abas) is already present at the rostromedian acroterminal domain (sparsely at E11; Fig. 8a–c and better developed at E11.5; Fig. 8d, e). Its prospective bilateral wings extending caudalwards under the optic stalk are still underdeveloped. There are fewer hp1 posterobasal and p3tg cells (pbas; p3tg). In contrast, the p2tg, nflm, and rtg cell groups in the caudal diencephalon and the m1 midbrain unit are much more populated, and differentiation has started to expand into the thalamic, pretectal and m1 alar plate. A few basal cells are present even in the retarded m2 midbrain unit (m2; Fig. 8b). It is unclear whether the oculomotor nucleus is present at these stages within m1, but its earliest cells might be found next to the floorplate (3; fp; Fig. 8b).

At E12 (Fig. 9a) the earliest hypothalamic basal groups (abas, pbas) and the prethalamic p3tg group are practically confluent, but still less massive in appearance than the p2tg, p1tg, and rtg groups that follow caudalward (note at the dp1 basal domain we have changed the name from nflm into p1tg; this is because p1tg surely contains additional populations apart of the precocious nflm component). Ventrally to rtg we now clearly see the oculomotor nucleus (3; Fig. 9a). In addition, there emerges now a separate hypothalamic hp1 basal group, placed ventral to pbas. It clearly corresponds to what was identified as the *periretromamillary area*, a.k.a. "posterior hypothalamic area," which characteristically expresses *Otp* and *Sim1* genes (prm; Fig. 9a) [Puelles et al., 2012a]; the underlying *retromamillary area* (rm) is still wholly undifferentiated at E12. Interestingly, some AChE-positive p3tg cells seem directly continuous with prm (Fig. 9a–c), bespeaking of a common dorsoventral subdivision of the basal plate. At

E13.5 and E14.5, this new hypothalamic basal band expands into hp2, forming the *perimamillary area* (pm; Fig. 9b, c) [Puelles et al., 2012a]. The underlying prospective *mamillary area* (m) remains undifferentiated at these stages, similarly as the rm. The extensive hypothalamic *tuberal area*, which lies intercalated between the abas and the pm, also remains unpopulated (tu; Fig. 9b, c).

### D.2 – Alar Plate

At E11/11.5 the pretectal alar plate (dp1) is populated in both its commissural and precommissural parts, with predominance of the former, as seen in the chick and lizard (cpt; pcpt; Fig. 8a–d). The thalamic alar plate shows incipiently an anterobasal population (ab; Fig. 8b–e) as well as a ventrocaudal cell group tentatively tagged hl? that seems to translocate in following stages along the retroflex tract (rf) course into the *lateral habenular area*. In Puelles et al. [2015b] we postulated that this ventrocaudal thalamic cell group may represent a ventrodorsally migrating population targeting the lateral habenular area (hl?; Fig. 8b–e; see also HL?; rf; Fig. 9a–c). At later stages the ab and hl? populations become more distinct, but the rest of the thalamic population, developed between E13.5 and E14.5 shows only weak to medium levels of AChE reaction in a ventrodorsal gradient (th; Fig. 9b, c). The ventralmost thalamic portion was interpreted to represent the primordium of the medial geniculate nucleus, known to have the earliest birthdates (MG; Fig. 9c) [Altman and Bayer, 1988].

The m1 alar midbrain displays at E11/11.5 a ventral population of AChE-positive neurons; we believe that rather than to the tectal grey or superior colliculus these belong largely to the Me5 population, since in mammals such singular cells adopt preferentially an initial ventrolateral position within the m1 and m2 alar domain (coinciding with the descending course of the mes5 tract) [see Puelles et al., 2015b]. This presumably occurs after migrating there out of an initial position adjacent to the roof plate (the locus where this population appears in sauropsids and other vertebrates). Moreover, similar cells seem to cross caudalward the m2 and isthmic boundaries, invading the prepontine alar hindbrain (r0 and r1); in the adult mouse and rat Me5 neurons are found mainly in the caudal lateral midbrain and at alar r0 and r1 prepontine sites, lateral to the locus coeruleus; none penetrate r2; they are always disposed along the me5 tract, whose dendritic branches enter the trigeminal root in r2. We interpret this temporospatial pattern as a caudal migration of some Me5 elements into the hindbrain. It apparently occurs only in mammals. This Me5 migratory phenomenon



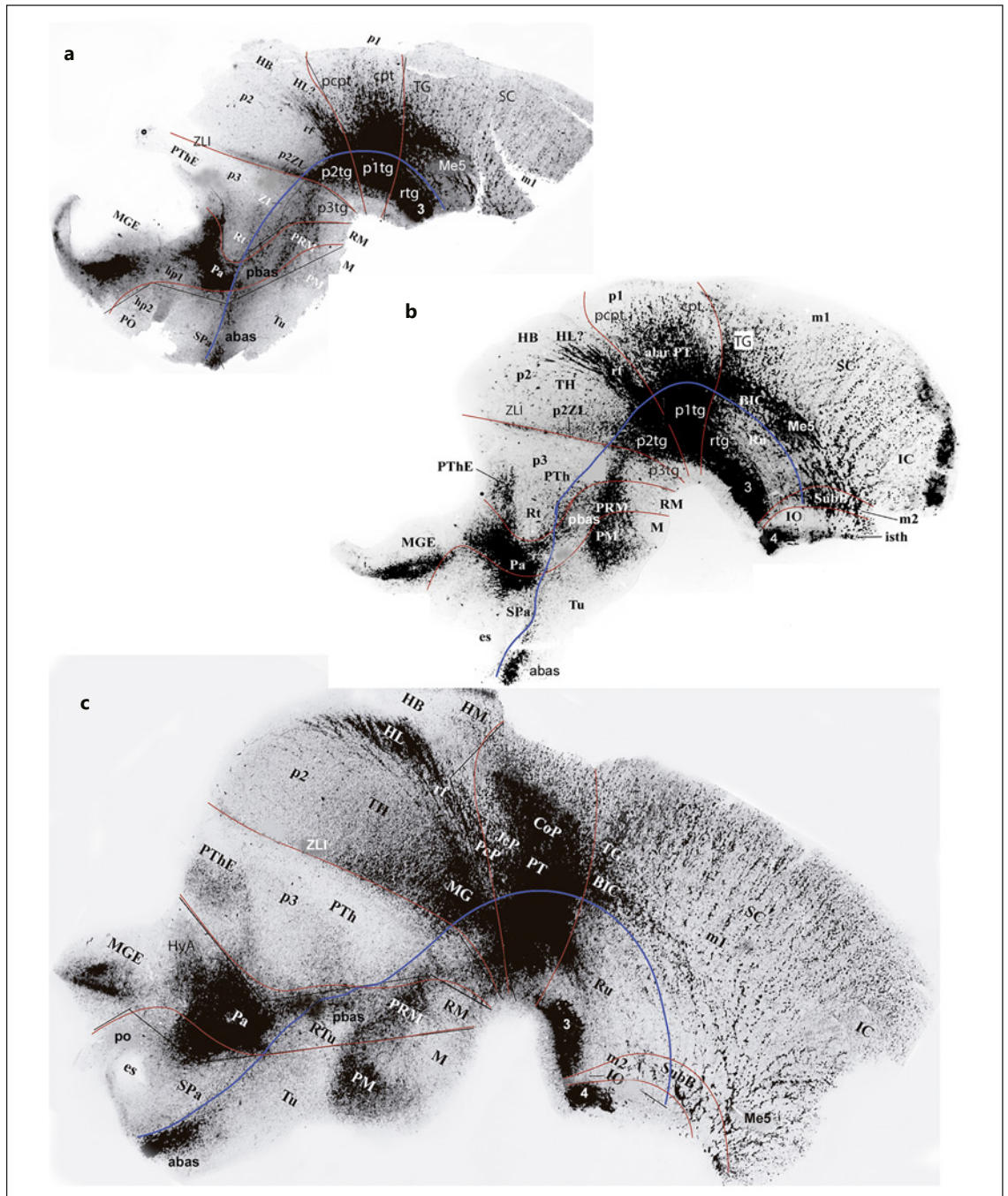


**Fig. 9.** AChE-reacted flat mounted rat forebrain specimens at E12 (a), E13.5 (b), and E14.5 (c) (rostral to the left). At these stages we see the superior colliculus (SC) m1 population (homologous to sauropsidian tect) emerge and develop, distinct from the rostral more advanced tg area and the caudally less advanced inferior colliculus (IC; homologous to the sauropsidian torus semicircularis, or tor). The singularly placed Me5 population continues present. The pretectum also shows more advanced populations. The thalamus reveals the ascending hl? population, which reaches the habenular area at E14.5 (HL; c). Note the relationship with the retroflex tract (rf). The prethalamus shows little AChE reaction, except

at its dorsal eminential portion (PThE; see b, c). The hypothalamic basal domain is much enlarged in surface, allowing progressive visualization of the periretromamillary and perimamillary band (PRM, PM) forming a capsule dorsal to the undifferentiated retro-mamillary and mamillary regions (RM, M) next to the floorplate (incipient in a; more advanced in b and c). The alar hypothalamic Pa area is also large and displays intense AChE activity. Not so the SPa area. The hypothalamo-amygdalar corridor (HyA) that puts Pa in contact with the telencephalic pallial amygdala is seen in a [see Garcia-Calero et al., 2008]. AChE reaction is evident in the subpallium (MGE), but not significantly in the preoptic area.

is already apparent at E11 and E11.5 (Me5; Fig. 8b, d; 10b), and can be corroborated likewise at E12, E13.5, and E14.5 (MeV; Fig. 9a–c; 10a). The m1 domain corresponding to the presumptive tectal grey and superior colliculus (tg; sc; the latter is homologous to tect in sauropsids) shows dorsoventrally arranged linear arrangements of AChE-positive neurons from E12 onwards (sc; Fig. 9a–c). Rostrally, the presumptive *tectal gray* formation (tg) shows higher cell density (tg; Fig. 9a–c). Caudally, the primordium of the inferior colliculus, the mammalian homolog of the sauropsodian tor, displays a more retarded status (ic; Fig. 9a–c).

The rat alar prethalamus is surprisingly poorly populated by AChE-positive cells, particularly when compared with the lizard counterpart (Fig. 7). Hardly any cell is visible at E11/11.5 (Fig. 8). At E12, E13.5, and E14.5 the only clear prethalamic alar differentiation affects the hyperdorsal *prethalamic eminence*, which characteristically lines caudally the primordium of the interventricular foramen (E; Fig. 9a–c). The underlying *central* and *subcentral* prethalamic subdomains (C; SCe; Fig. 9a–c) [Puelles et al., 2021] only show here or there very pale AChE reaction, possibly artefactual (e.g., insufficient cleaning of mesenchyme before the reaction), or else indicative of a local chemoarchitectonic singularity (lack of AChE activity), rather than implying an absence of neurogenesis and differentiation. We know that the prethalamic eminence population is born later than the underlying central and subcentral ones [Puelles et al., 2021].

The alar hypothalamus is largely unpopulated at E11/11.5 (Fig. 8), but soon develops thereafter the highly populated *paraventricular area* (Pa), which develops first within the peduncular hypothalamus (hp1) and then in the terminal hypothalamus (hp2; extending into the optic stalk area) (Pa; Fig. 9a–c). Part of the Pa population extends into the amygdalar area of the telencephalic pallium along what we have recently named the *hypothalamo-amygdalar corridor* (HyA; Fig. 9a, c) [García-Calero et al., 2021]. The paraventricular area is separated from the alar-basal boundary by a less progressive *subparaventricular area* (SPa), also distinguishable partially immediately above the abas/pbas (hp2, hp1) basal formations (SPa; Fig. 9a–c). The *preoptic area* only shows very weak background AChE activity, similarly to the central/subcentral prethalamus, possibly indicating again lack of efficient AChE reaction or that rat preoptic neurons do not express the enzyme. Instead, a distinct patch of AChE expression is found from E12 onwards at the growing *medial ganglionic eminence* of the telencephalic subpallium (po; MGE; Fig. 9a–c).

## E – Hindbrain Patterns

E.1 – We start this description with two glimpses at the rat hindbrain reacted for AChE at E11.5 and E14.5 (Fig. 10a, b). The lateral view at E14.5 illustrates a relatively advanced stage in which all rhombomeres (r0–r11) are already partially populated. The *prepontine*, *pontine*, *retropontine*, and *medullary* proneuromeres (PrP, P, RP, Med; compare Fig. 1b, c) are marked by red interrhombomeric boundaries (Fig. 10a). It can be seen that some aspects of the rhombomeric neurogenetic modes are subtly characteristic of the respective proneuromeres, though r6 rather resembles the Med elements and r5 perhaps the P elements. The rostral PrP domain is also known as the “isthmocerebellar region” (r0 builds the cerebellar vermis, while r1 forms the cerebellar hemispheres and floccles). The sum of r0 and r1 is patterned by the agency of the morphogen FGF8 released from the *isthmoc organizer* at the isthmo-mesencephalic border (compare this AChE-negative area in the rat with the positive isthmoc organizer neuroepithelium seen in the lizard; Fig. 7).

As commented above, in mammals, the PrP domain is selectively invaded by Me5 neurons migrating caudward from the midbrain. This phenomenon is captured at E11.5 (Me5; Fig. 10b), jointly with the earliest ventral premigratory stages of development of the branchiomotor trigeminal and facial motor populations at r2–r3 and r4, respectively (5; 7; Fig. 10b). The paired rhombomeres r2 and r4 are advanced in neurogenesis compared to the other rhombomeres. The branchiomotor motoneurons are born at paramedian ventral sites (Fig. 10b) but ultimately migrate tangentially into the closest part of the alar plate (case of the trigeminal nucleus; 5 across r2 and r3). The facial motoneurons instead first migrate from their birthplace in r4 caudalwards into paramedian r6 (captured in Fig. 10a; migr 7 across r4–r6) [see Studer, 2001], before moving into the alar plate (5 in r2 and r3; Fig. 10a) [see Windle and Austin, 1936; Heaton and Moody, 1980; Moody and Heaton, 1983a,b; Ju et al., 2004; Puelles et al., 2019b].

The alar-basal boundary is not easy to visualize in AChE wholemount preparations at these stages. We traced in Figure 10a a blue line indicating tentatively this boundary, judging mainly by the known postmigratory position of the mouse trigeminal motor nucleus [Puelles et al., 2019b]. Various other cell populations seem to translocate from the basal plate into the alar plate, or vice versa. At E14.5, the hindbrain sensory columns are not yet significantly developed (Fig. 10a).

E.2 – We next present chick embryo material from the thesis of Amat [1986]. Open-book flattened hindbrain

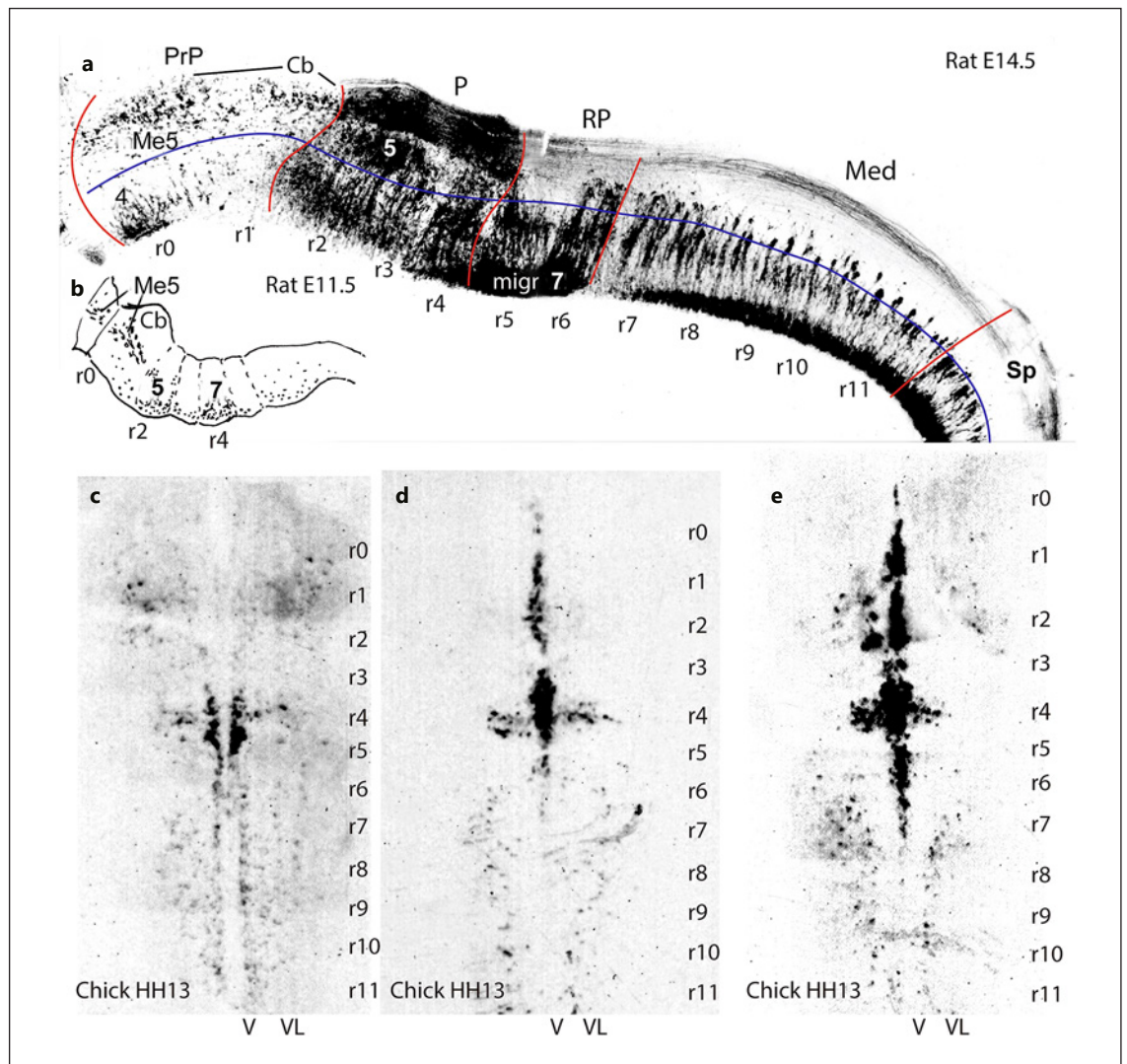


**Fig. 10.** AChE-reacted wholemounts of rat hindbrain (**a, b**; rostral to the left) and flattened chicken hindbrain opened as a book (**c–e**; rostral upwards; floorplate central). **a** Lateral view of the rat hindbrain at E14.5 (compare with the lizard hindbrain in Fig. 7b). The proneuromeres PrP, P, RP, and Med are limited by red lines; the rhombomeres are identified underneath; the estimated alar-basal boundary is represented by a blue line. At PrP levels neurogenesis is retarded; the trochlear motor nucleus (4) appears in the isthmial (r0) basal plate, which is sparsely populated in r1. In the alar plate there are migrated Me5 cells from the midbrain and the earliest cerebellar neurons in r1 (Cb); they correspond to the prospective cerebellar nuclei. At P levels (r2–r4) we see the most advanced part of the hindbrain, particularly r2 and r4. Note these 3 units also show advanced alar neurogenesis. The trigeminal motor nucleus population (5) has already finished its migration into the alar plate. The facial motor nucleus cells that originated in basal r4 are in the

process of migrating caudalward into r6 (migr 7). The latter neuromere has some alar neurons, similarly as all the rhombomeric units composing the Med region (r7–r11). Inside the basal plate, “ventral” and “ventrolateral” neurogenetic zones can be distinguished (not marked). In all rhombomeres except r0 and r1 many neurons seem to be moving between the basal and alar domains. **b** This is a drawing from an E11.5 rat hindbrain specimen viewed laterally. The precocious basal plate cell groups in r2 and r4 (presumably the future 5 and 7 motor nuclei) are seen. The migration of Me5 cells into r0 and r1 is in course. **c–e** Three examples of AChE-reacted chicken hindbrain flattened in open-book form after cutting the roofplate. The rhombomeres r0 to r11 are indicated. The letterings V and VL at the bottom right of each specimen refer to “ventral” and “ventrolateral” neurogenetically active zones along the dorsoventral dimension. Note subtle progressive changes from **c** to **e**. Note r3 is quite small at the beginning.

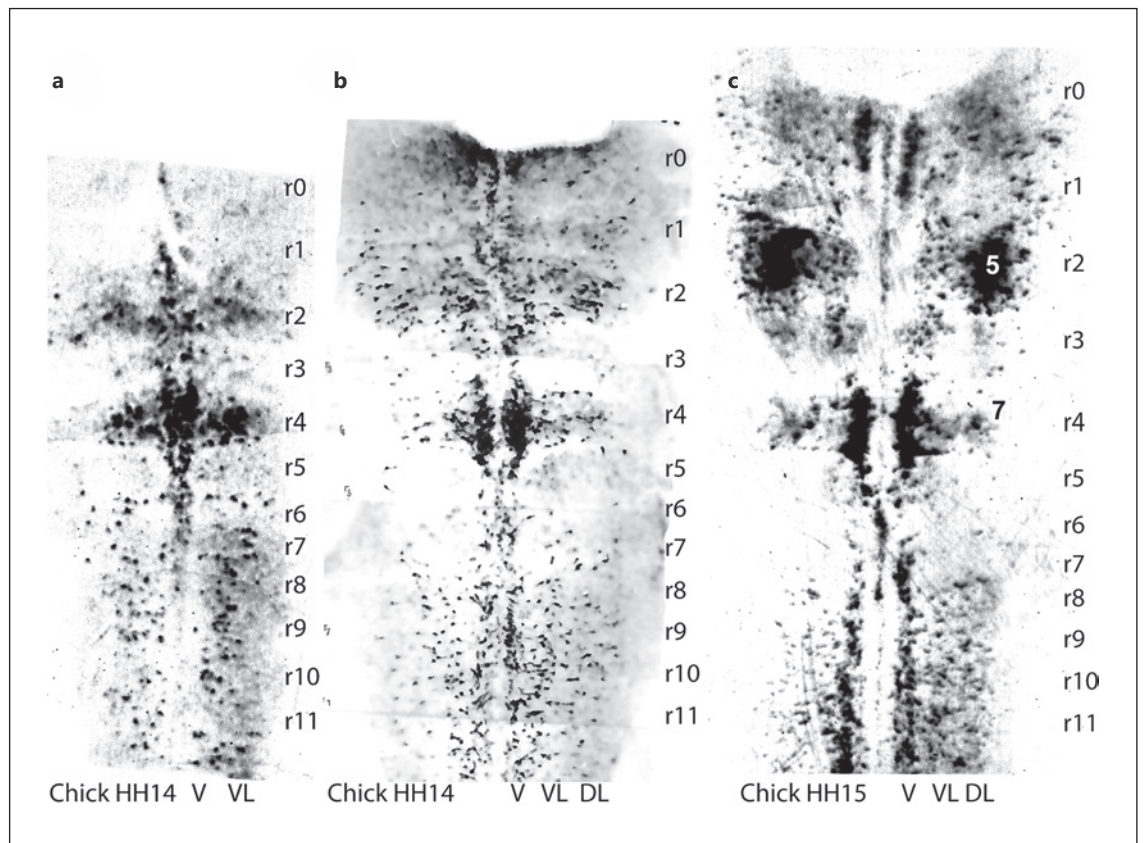


**Fig. 11.** Open-book AChE-reacted wholemounts of chicken hindbrain at stages HH14 (**a**, **b**) and HH15 (**c**). The markings are as in the previous Figure (now adding the DL – dorsolateral – neurogenetic zone at the bottom). Observe across **a–c** the progression of the trigeminal migration from the ventral basal plate into the alar plate (5 in **c**). Birds lack the caudal migration of facial motoneu-

rons born in r4 observed in mammals and other vertebrates (shown in Fig. 9a, b; 10a, b), but they do migrate into the r4 alar plate (7 in **c**). Imminent production of the trochlear neurons is apparently announced by neuroepithelial AChE-positive ventral paramedian positive bands at r0 level (**b**, **c**).

wholemounts at diverse stages from HH13 to HH22 are illustrated here (Fig. 10c–e, 11–14); the original thesis also shows non-flattened wholemounts and abundant sectioned material. Our present hindbrain specimens are all shown aligned mutually at the level of r4, and the obvious neuromeric levels are identified for cross-comparison of the stages. At the bottom of each image there is a code that roughly classifies topographically the sites where neurons are found as *ventral*, *ventrolateral*, *dorsolateral*, and *dorsal* zones (V, VL, DL, D; these are roughly based on Hugosson [1957]); eventually an approximate alar-basal boundary area emerges between VL and DL as a longitudinal cell-poor *gap* – it is coded correspondingly (G). At early stages only V and VL domains are populated, followed in successive steps by DL and then D domains. Note that at most stages except the last studied a number of cells seem to be in the process of

moving mediolaterally between these four zones, even crossing the alar-basal boundary, as was mentioned above.

The earliest differentiating hindbrain neurons appear at stage 9, placed along the VL area of the neural wall corresponding to prospective r7–r11 (that is, proneuromere Med; not shown) [see Amat, 1986]. Such precocious cells continue to develop in the subsequent stages, adding corresponding V components (not shown). At stage 13 sparse and relatively weakly labelled medullary V and VL populations are well visible extending from r7 to r11 (Fig. 10c–e). Earliest AChE differentiation in more rostral proneuromeres occurs in caudal pontine r4 at stage 13. We show 3 examples of that stage side by side, due to their subtly progressive appearance (r4; Fig. 10c–e). The V group of r4 appears as a linear arrangement of strongly positive cells next to the negative floorplate (note this

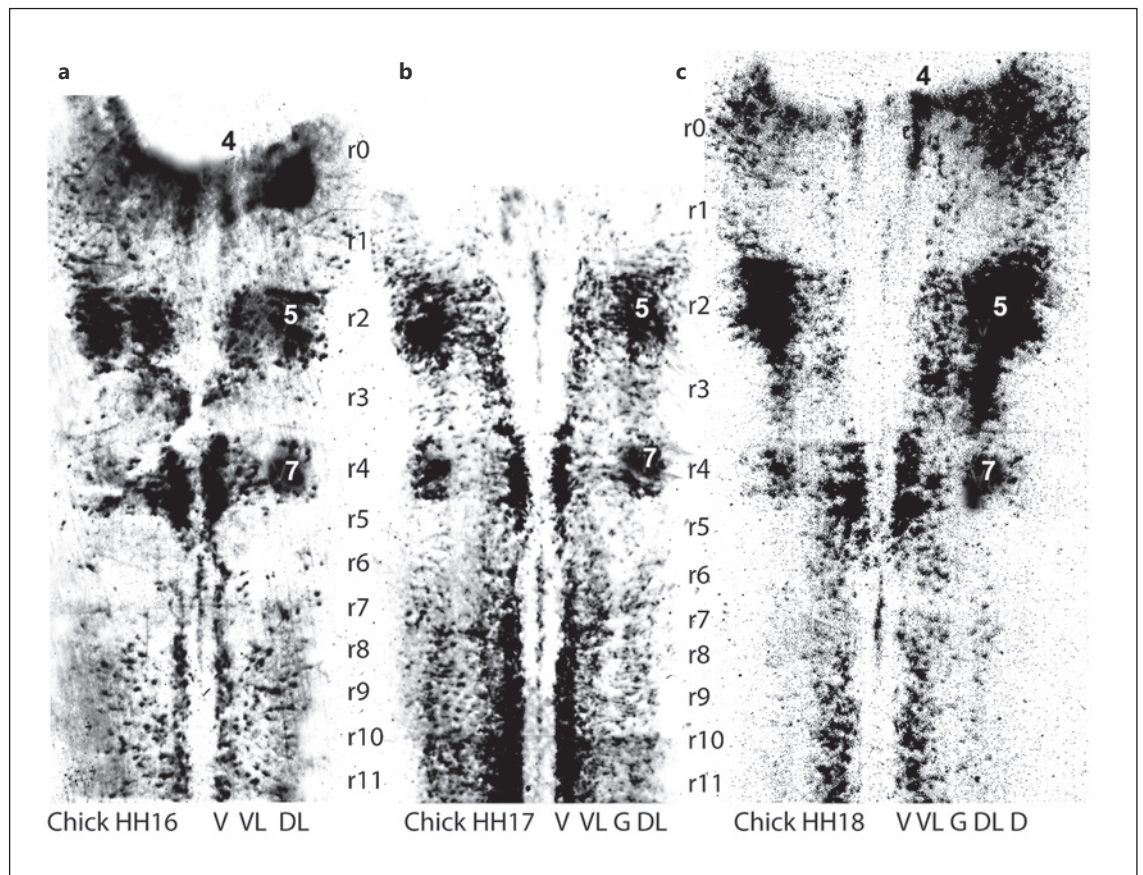


**Fig. 12.** Open-book AChE-reacted wholemounts of chicken hind-brain at stages HH16 (**a**), HH17 (**b**), and HH18 (**c**). The markings are as in the previous Figure (now adding the D – dorsal – neurogenetic zone at the bottom, as well as the alar-basal gal – G, both first observed at stage 18). These stages mainly illustrate the re-

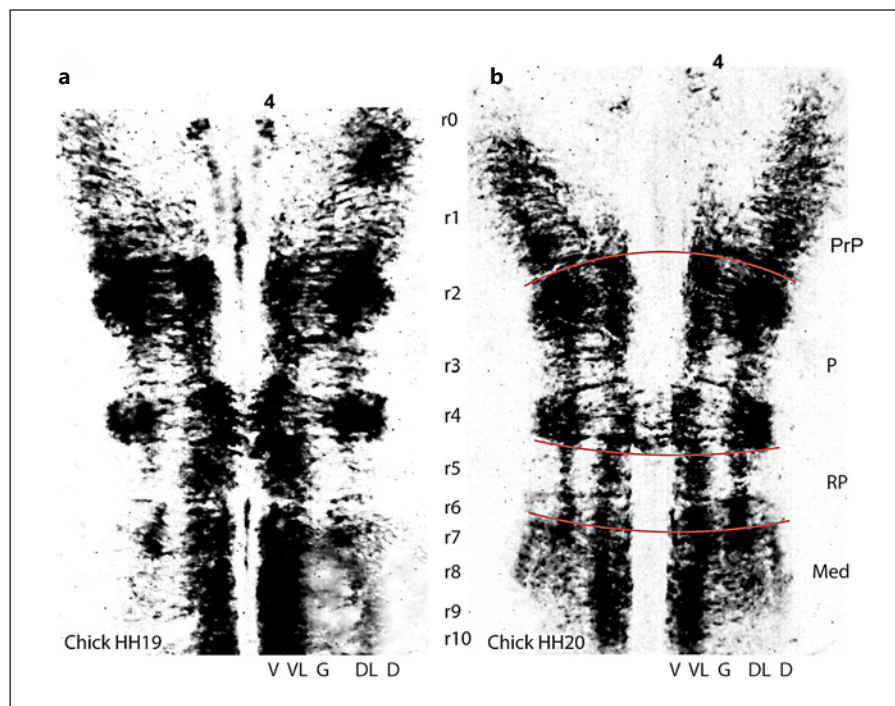
tarded advance of the different neurogenetic zones in the unpaired rhombomeres (notably the r3 part of the migrated trigeminal motor nucleus; **c**). The trochlear motor nucleus (4) appears in the isthmus or r0 (**a, c**). The “dorsal” neurogenetic zone first appears at r4 level.

rhombomere is trapezoid in shape, being longer at V than more dorsally) [Vaage, 1969]. Across the three examples shown in Figure 10c–e we see that r4V apparently produces a number of laterally (dorsally) migrating neurons, which momentarily occupy the VL locus (these cells probably represent the earliest primordium of the facial motor nucleus, equivalent to the rat ones shown in Fig. 10b). The specimen in Figure 10d shows additionally a similar r2V group, but without any sign of lateral migration, while the specimen in Figure 10e shows an incipient lateral migration into r2VL particularly at its left side, as well as further strongly labelled V group neurons at r1 and r5–r7. Simultaneously, dispersed r7 and r8 VL cells increase markedly in number (Fig. 10e).

At stage 14, medullary (r7–r11) populations and r4 and r2 cell groups still predominate compared to the retarded rhombomeres r0, r1, r3, r5, r6 (Fig. 11a, b). The

second stage 14 specimen shown in Figure 11b seems slightly more advanced, notably showing earliest development of DL neurons within the medullary field (r7–r11), as well as more advanced lateral migration of trigeminal motoneurons from V into VL in r2. At stage 15 (Fig. 11c) most of the migrated facial and trigeminal motoneurons seem to reach the DL region of r4 and r2, respectively, that is, they arrive at the prospective alar plate (5; 7; Fig. 11c), though the respective migrating streams are still evident. Interestingly, the r2V group practically disappears between stages 14 and 15, implying that its elements have moved entirely into VL and DL (compare Fig. 11b and c). In contrast, the r4V group persists at stage 15. Ulterior observations suggest that this is due to a second r4V cell population apart of the facial motoneurons, which will later migrate selectively across the r4 midline floor. In the meantime, a r3V group appears and better

**Fig. 13.** Open-book AChE-reacted whole-mounts of chicken hindbrain at stages HH19 (a) and HH20 (b). The markings are as in the previous Figure. At these stages we see progress in the alar plate and the basal V and VL zones tend to fuse together (and expand rostralwards into r1). The DL neurogenetic zone of the retarded rhombomeres increasingly becomes active, and the D zone expands into r2, r3 (tenuously), r4, r6, r7, and r8. The isthmus trochlear nucleus (4) starts to become rounded (a). Note migration across the midline at r4 of the vestibular efferent neurons.



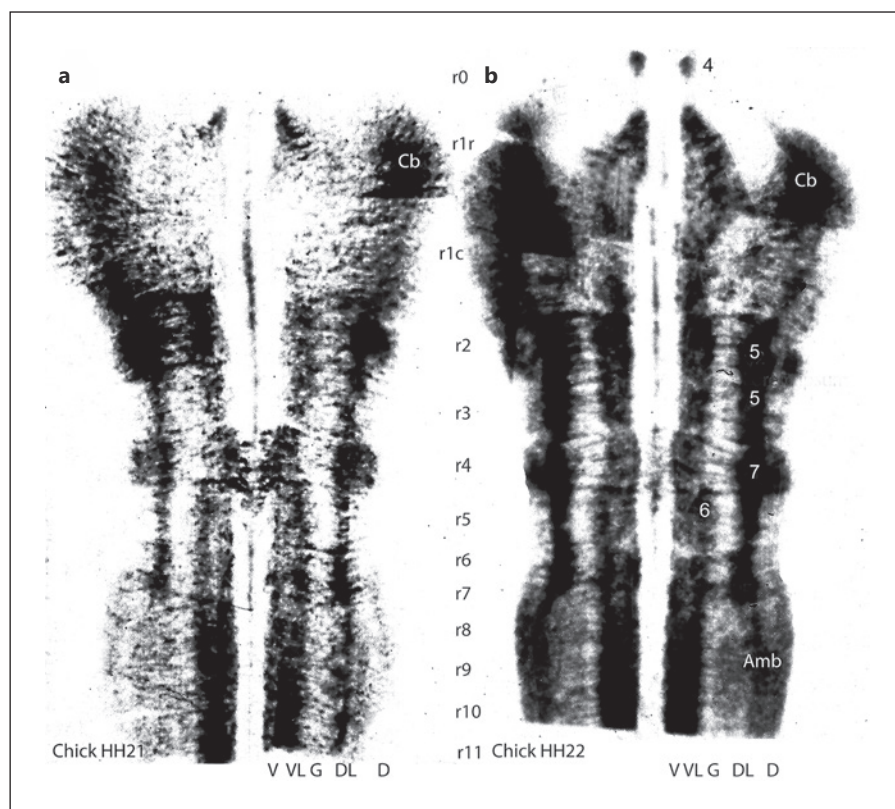
developed V groups are seen at r5 and r7, extending as well into r8–r11 (Fig. 11a–c). Figure 11b and c also show that r0 starts its neurogenetic activity in this period at V, VL, and DL sites (compare Fig. 11a), contrasting with the relatively more retarded r1 rhombomere. The floorplate also starts to express neuroepithelial AChE at its median radial glia, apparently also in an heterotopic heterochronic pattern (Fig. 11c).

Over stages 16–18 (Fig. 12a–c) rhombomeres r1, r3, and r5 continue visibly retarded in their overall neurogenetic development compared to the other neuromeric units. In the precocious medullary region (r7–r11) the earlier V and VL cell groups tend to coalesce into a V/VL complex that represents the core of the basal plate (either addition of more neurons filling the V-VL gap or cell movements from VL cells aggregating into V may be involved in this process). Simultaneously, at stages 17–18 a distinct longitudinal cell-poor gap emerges (best seen at medullary levels) that separates VL from DL (G; Fig. 12b, c; this may coincide with a displacement of VL cells ventralwards into compacted V/VL). The new gap plausibly contains the theoretically lineal alar-basal boundary, insofar as we know it limits with the branchiomotor nuclei 5 and 7 migrated into the alar plate, jointly represented by the DL and D regions (Fig. 12b, c) [Ju et al., 2004]. Its relative lack of AChE-positive cells at these and immedi-

ately subsequent stages suggests that the corresponding G progenitor cells (possibly including the dorsalmost basal molecular microzone and the ventralmost alar microzone) are relatively retarded in neurogenesis (obviously, the gap will become filled with neurons later). The beginning of a differentiating D subregion clearly appears at stage 18 in r4 (dorsal to the DL zone containing the 7 motor nucleus) and less markedly in r2 (dorsal to the 5 motor nucleus and associated DL) (Fig. 12c). The ventral (V) cell group at r0 level possibly represents the primordium of the trochlear motor nucleus (4).

At stages 19 and 20 (Fig. 13a, b) the relatively retarded neuromeres r1, r3, r5, and r6 show significant advance in their neurogenetic process, by which they imitate the more advanced counterparts, thus achieving gradual columnar coherence at least at V and VL (basal plate) levels. We delimited in Figure 13b the proneuromeres PrP, P, RP, and Med with red transversal lines, to help visualizing similarities and dissimilarities. The alar DL region appears still somewhat retarded at r1, r3, r5, and r6 at stage 19 (Fig. 13a), but advances considerably by stage 20 (Fig. 13b). Interestingly, some interrhomomeric boundaries appear marked by local accumulation of differentiated neurons, for instance at the r3/r4 and r5/r6 limits (Fig. 13b). At these two stages the previously incipient D cell groups are better developed in r2 and r4 and have

**Fig. 14.** Open-book AChE-reacted whole-mounts of chicken hindbrain at stages HH21 (**a**) and HH22 (**b**). The markings are as in the previous Figure. Note the distinct appearance of a poorly populated gap between VL and DL (marked G at the bottom), roughly including the linear locus of the alar-basal boundary. This suggests the gradual end of mutual transfer of cells between the basal and alar plates. The final part of the migration across the r4 midline appears only in **a**. Rhombomere 1 results divided into rostral and caudal parts (r1r and r1c), whose r1r basal plate domain appears more precocious (**a, b**). The cerebellar plate (Cb) in r0 and r1 also shows significant advance. The branchiomotor cell groups 5 (in r2 and r3), 7, and ambiguous (Amb) that migrated to the alar plate are labeled in agreement with earlier analysis [Ju et al., 2004]. Note also AChE-positive labeling of midline radial glia of the floor-plate.



started to appear as well in r7 (stage 19; Fig. 13a), extending next to r8 (stage 20; Fig. 13b). It is unclear whether r1 and r2 also develop incipient D cell groups at stage 20.

The well-known migration of efferent vestibular neurons across the midline floor domain of r4 becomes visible in our material between stages 19 and 21, that is, and the migration roughly ends at 3 days of incubation (Fig. 13a, b; 14a) [Fritzsche et al., 1993; Tiveron et al., 2003]. They represent the remnant of the r4V cell group that did not follow the branchiomotor facial motoneurons into the alar plate in previous stages, persisting transiently in a V topography.

Finally, at stages 21 and 22 (Fig. 14a, b) both the basal plate column (represented by aggregated V/VL cells) and the alar plate column (sum of DL and D cells) become increasingly coherent, as the retarded rhombomeres attain levels of initial dorsoventral differential maturation displayed first by the advanced hindbrain segments. The change is clearly observable across r1, whose total length also seems to have increased in the meantime (possibly due to its previous relative lack of neurogenesis, which allows for more surface growth). This growth possibly explains the subdivision of r1 into rostral and caudal r1 companion parts (r1r, r1c; Fig. 14a, b) [Vaage, 1969, 1973;

Alonso et al., 2012; Puelles, 2013]. A distinct cone-shaped VL cell group (present at stage 21 in r1r but not in r1c, where something similar emerges at stage 22) may correspond to the prospective *dorsal and ventral tegmental nuclei*, typical basal structures restricted to r1r (Fig. 14a, b) [Puelles et al., 2019a]. Note r1 does not produce motoneurons, but still develops a distinct V cell group besides the VL area. This r1V domain extending also into r0 may include prospective serotonergic raphe nuclei, which are produced in a thin paramedian band [Alonso et al., 2012].

At these stages corresponding to 3 days of incubation, the alar-basal cell-poor gap clearly extends into the rostral preontine hindbrain, although many transverse cell bridges are observed that interconnect basal with alar regions. The D alar subregion is now seen practically in all rhombomeric units (Fig. 14b).

## Discussion

The prosomeric model employed in this analysis was presented and partly justified in the Introduction; see also in this respect our Figures 1, 8f, and 15, which are practically self-explanatory. Discussion about the sensibility

and specificity as a neuronal marker of AChE whole-mount histochemistry was treated in considerable detail in Puelles et al. [1987a] and Puelles et al. [2015a]; this will not be repeated here. We also avoid for simplicity a detailed discussion of the literature on neurogenetic patterns in these or other types of vertebrates (e.g., the results obtained by cited authors using reduced silver, or various histochemical, chemoarchitectonic or autoradiographic methods), because no earlier study reached the level of detail and descriptive precision obtained in the present occasion. This was largely due to the stronger analytic properties of the morphological model employed here (the updated prosomeric model) over previously used models, so that a discussion of alternative descriptions would need to delve constantly on the defects in the respective models and approaches that impeded other authors to interpret properly their available material. This would distract us from the observable pattern of neurogenesis itself, which is our major interest. Readers can and probably will try their hand at guessing how our set of data would have been described by other authors using, for instance, the conventional columnar model of the diencephalon (e.g., how would they deal with our forebrain basal plate, or with the ZLI?). If the neuromeres and their subdivisions do not help understanding the comparable (homologous) complexity of neurogenesis in different species, what other concept does? We will thus center our discussion on the heterochronic neurogenetic patterns.

#### *Corroboration of the Prosomeric Model*

It is an immediate conclusion of our present comparative study that the heterochronic development of the longitudinal basal plate band in the forebrain of sauropsids and mammals supports fully the concepts of “forebrain basal plate” and “forebrain alar-basal boundary” initially proposed by His [1893, 1895, 1904]; these earlier notions later became also tenets of neuromeric theory. The number of brain tagmata, proneuromeres, and neuromeres predicted by the updated prosomeric model results strongly corroborated by our findings on heterochronic neurogenetic behavior along both the basal and alar plates. This pattern has been progressively adjusted in the forebrain and extended into the hindbrain over the years since Puelles and Rubenstein [1993]. The basal plate band and the alar-basal boundary extend throughout the brain in parallel to the floor plate, alar plate, and roof plate, representing an obvious manifestation of shared dorsoventral patterning throughout the brain, with local heterochronic differentiations. All these longitudinal structural elements converge rostrally upon the acroterminal do-

main first postulated by Puelles et al. [2012a] and further described by Puelles and Rubenstein [2015] and Puelles [2017]. It is thus easy to conclude that our collection of wholemount results does not support *any* concept of the forebrain axial structure that is held to end in the telencephalon [e.g., Herrick, 1910, 1933, 1948; Kuhlenbeck, 1973; Altman and Bayer, 1995; Swanson, 2012]. This is not the place to mention the multiple corroborating findings based on differential gene expression and mutant phenotypes that equally support this conclusion.

The updated prosomeric model essentially deals with tagmata, proneuromeres, and individual neuromeres throughout the brain, subdivided dorsoventrally into *shared fundamental longitudinal zones or areas* [see Nieuwenhuys and Puelles, 2016; Nieuwenhuys, 2017] (this common aspect is actually what adds the property of “metamery,” i.e., conceptual *repetitive structure*, to neuromeres, irrespective of any *differential* anteroposterior molecular specification or heterochronic regulatory aspects the neuromeres may display). Our present data in sauropsids and mammals further suggest that mere distinction of major (primary) floor, basal, alar, and roof developmental subdomains of each neuromere is not *sufficient* to account for the detailed microzonal level of regionalization observed in the brain; for instance, the precocious basal areas do not emerge suddenly as wholly populated domains, but start neurogenesis at their respective dorsal ends and thereafter expand ventralwards. Puelles [2013] reexamined in general this notion as regards differential *dorsoventral (DV) subdivisions*, which are best known molecularly and causally at the spinal cord and hindbrain tagmata. There is a consensus that there may be 6 DV alar subdivisions and 5 basal ones across these tagmata, and nothing impedes in principle that this may be a general rule across the whole brain, that is, *mutatis mutandis*, in the forebrain. Puelles et al. [2012a, b] considered the situation at hypothalamic and midbrain levels without deriving definitive numeric conclusions, but found that multiple dorsoventral subunits of both basal and alar plates do exist at both places, thus suggesting a shared forebrain tagma pattern comparable at least generally to the hindbrain and spinal patterns. Present results – particularly those in the rat – corroborate point to point the major mouse alar and basal hypothalamic DV subdivisions defined molecularly by Puelles et al. [2012a].

A theory contemplating *secondary organizers*, *morphogen diffusion*, and *genomic read-out of positional information* has been developed in recent years which provides fundamentals to understand how such secondary regionalization of the alar and basal plates may occur,

regulated independently (differentially) within the neuromeres (reviewed in Puelles [2017]). The same theory admits not only intraneuromeric dorsoventral subdivisions but also *anteroposterior zonal subdivisions*, which may occur independently at alar or basal sites. Relatively well-studied examples of such AP patterning inside a neuromere can be found in the work of Ferran et al. [2007, 2008, 2009] on the pretectum, and in that of Puelles et al. [2021] on the prethalamus. Other published studies also deal with the thalamus or the midbrain. Our present data likewise provide multiple corroboration of these concepts. It is remarkable that we rarely found neurons appearing in a *temporo-spatial gradient within particular intraneuromeric alar microzonal areas*. The initial neurons usually were sparsely distributed over the corresponding area and their density increased subsequently, sometimes *at different rates* in neighboring microzones (e.g., see the cases of Me5, tect, tg, and tor subareas in alar m1). This contrasts with the habitual description of gradient neuronal birthdates in autoradiographic neurogenetic studies. These discrepancies might be explained if these studies actually report an order manifested *between* microzones, rather than *inside* them (for instance, the conventionally described general rostrocaudal neurogenetic gradient over the tectal alar midbrain [LaVail and Cowan, 1971] might correspond to the order tg>tect>tor>preisth).

**Fig. 15.** Correlation of some gene expression patterns with the AChE neurogenetic pattern, consistent with the updated prosomeric model. **a** Expression of the gene *Dlk1* in the mouse at E13.5 (Allen Developing Mouse Brain Atlas) delineates uniformly the postulated *acroterminal forebrain domain*, which represents the linear rostral end of the neural tube. It falls inside the rostralmost prosomere (hp2; delimited by a red line) and extends from in front of the mamillary floorplate to in front of the end of the roofplate, at the locus of the septal anterior commissure (m, ac, se). It is divided into basal and alar parts by the rostral end of the alar-basal boundary (or the upper limit of the basal plate band – see **c**). Its morphological components can be checked in all vertebrates (see here the chick pattern in **c**). Note the ticker acroterminal median mantle zone corresponding to the precociously developing abas area. **b** Here the forebrain of a stage HH17 chick embryo was reacted with our standard double ISH protocol [Ferran et al., 2015] for expression of the genes *Shh* (dark reaction in the basal plate band, interthalamic ZLI and telencephalic preoptic area) and *Pax3* (weaker reaction seen in pretectum, midbrain optic lobe, and hindbrain alar plate; note *Shh* is expressed only in the floorplate of the hindbrain, leaving the basal plate negative). The topologic correspondence of the basal plate and ZLI expression of *Shh* with the location of the AChE-positive basal plate band is obvious. So is the correspondence of the preoptic *Shh*-positive patch with the area so

### *Causality of Observed Heterochronic Patterns in Neurogenesis*

In most cases, we still lack a full explanation of the observed heterotopic patterns of neurogenetic heterochrony revealed by wholemound analysis. As mentioned, analyses of proliferation patterns and neuronal birthdates in the brain, which might be informative, generally do not reach the precision needed by the observed interneuromeric and intraneuromeric patterning phenomena. This is an adverse effect of the long prevalence of the columnar model of Herrick [1910], which negated neuromeric phenomena, or even subdivisions within his own hypothetic columns. One rare exception in the autoradiographic literature is the study of chick isthmus nuclei by Puelles and Martínez-de-la-Torre [1987], done with the neuromeres in mind; we found that the cell birthday gradients of differently placed “isthmus” nuclei (some of which were not really in the isthmus neuromere) were restricted differentially to alar domains or subdomains of neuromeres m2, r0, and r1.

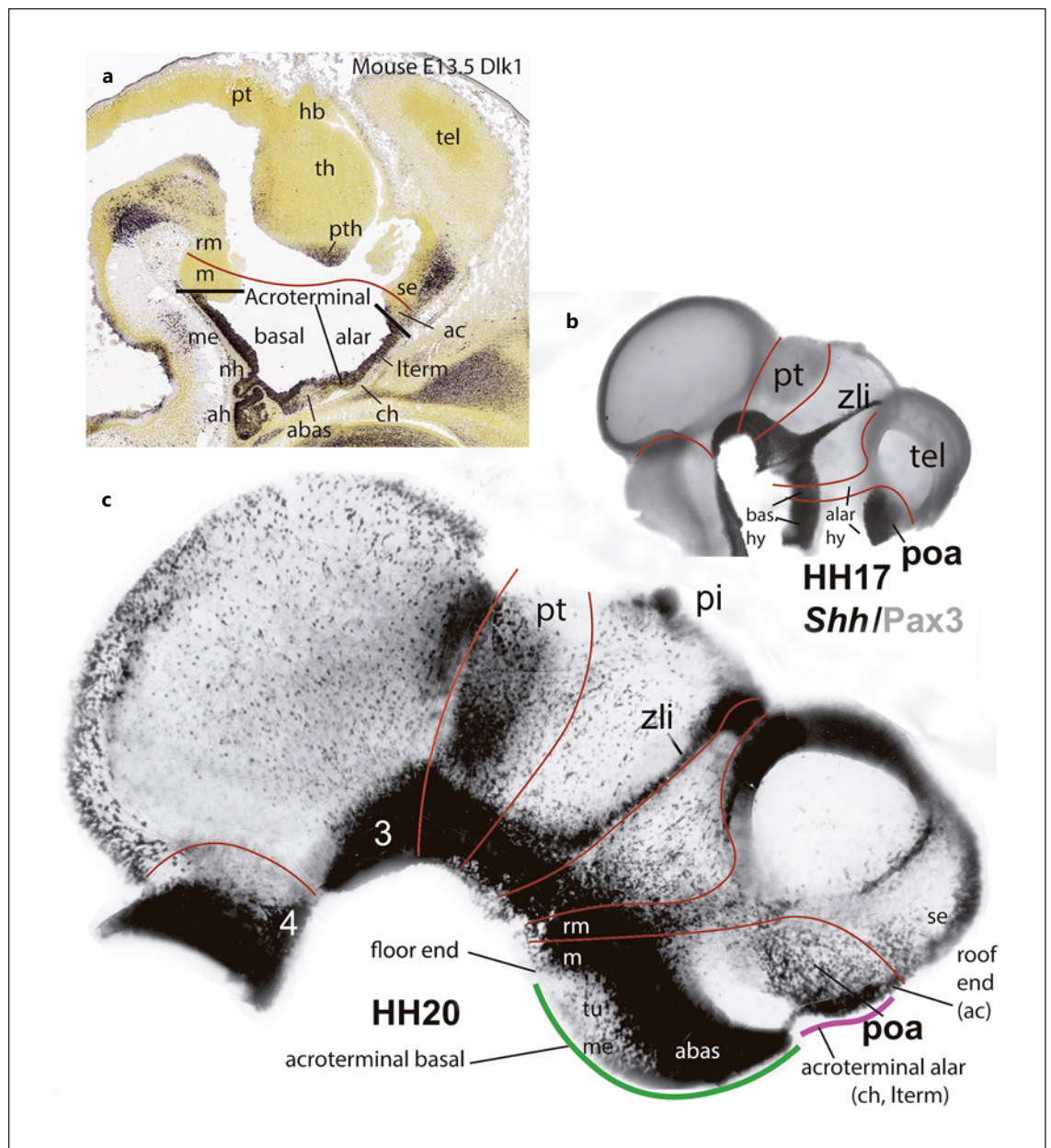
Studies dedicated to the differential neurogenetic mapping of brain areas that are known to subdivide secondarily in various directions, as occurs for instance with the “diencephalon columns,” the midbrain tectal vesicle, or the hindbrain dorsoventral columns, are practically absent. The autoradiographic diencephalon and hypothalamus rat studies of Altman and Bayer [1978, 1986,

identified with AChE. Since this gene starts acting earlier than the differentiation of AChE-positive features (already at neural plate stages), we may deduce that its activity at these sites is an upstream antecedent of the consequent AChE pattern (probably in combination with other genes). The *Pax3* pattern precisely delimits the rostral boundary of the pretectum (alar dp1) with regard to the thalamus (alar dp2). Finally, since *Shh* appears selectively in the basal hypothalamus and in the preoptic area (i.e., the non-evaginated subpallial telencephalon), the *Shh*-negative domain found in between across hp1 and hp2 corresponds to the alar hypothalamus. **c** We identified on this copy of the HH20 image with a thick green line the median extent of the basal acroterminal portion; this starts ventrally in front of the mamillary body (m), ascends across the tuberal median eminence (me) and neurohypophysis (not shown; compare **a**), and ends sharply at the alar-basal boundary jointly with the abas area. The alar part of the acroterminal domain is marked by a thick fuchsia line; it starts just above abas at the prospective optic chiasma (across the rostromedian alar hypothalamus; compare **a**, **b**), then ascends through the preoptic lamina terminalis to end just in front of the locus of the anterior commissure at the telencephalic septum (ch, lterm, ac, se). The red lines representing interneuromeric boundaries clearly are topologically orthogonal to all the longitudinal elements that co-define the axial dimension of the brain (floor, basal, alar, and roof plates).

(For figure see next page.)

1988, 1995] were interpreted aiming to obtain common overall gradients, and disregarded detecting neuromeric, alar/basal, or microzonal details of neurogenesis (none of these concepts were used). Such studies often were interpreted as showing one or several uniform cell birthday gradients (e.g., Angevine [1970] for the mouse diencephalon plus hypothalamus; LaVail and Cowan [1971] in the chick optic lobe; Creps [1974] for the preoptic and septal regions); even cortical studies have tended to unify results into large gradients rather than distinguish possible distinct adjacent fields [e.g., Bayer and Altman, 1991].

The molecular approach mapping developmental genes was clearly more productive in this regard. Often given genes were shown to be expressed precociously precisely where a distinct neurogenetic event occurred slightly later (e.g., the strictly *thalamic* expression of *Gbx2* preceding and restricted to the emergence of the main mass of thalamic neurons, but unrelated to histogenetically separate microzones such as the more dorsal *habenular* neurons, or the *anterobasal* thalamic subdomain) [Martínez-de-la-Torre et al., 2002]. Another clear-cut instance is the selective expression of *Otp* along the VL parts of the



15

hindbrain basal plate, as well as selective *Phox2b* expression at the V, DL, and D histogenetic zones [Ju et al., 2004; their Fig. 3f–h]. A review of some of these molecular correlations was offered in Puelles [2013; see also Puelles et al., 2004; Martínez et al., 2012; Puelles and Martínez-de-la-Torre, 1987]. Our present Figure 15b illustrates how an early pattern of *Shh* expression at the prospective forebrain *basal plate band*, *interthalamic zona limitans*, and *preoptic area* in the chick preconfigures, probably causally (since *Shh* codes for a diffusible morphogen, the SHH protein) [see Puelles, 2017], the shared early differentiation of AChE-positive neurons at these forebrain sites. The accompanying paler *Pax3* pattern in Figure 15b preconfigures the pretectum (plus the dp1/dp2 boundary) and midbrain alar domains, as well as the whole hindbrain alar plate (*Pax7* is also involved in this pattern) [see Ferran et al., 2015; Puelles et al., 2019b].

As regards the *molecular* dorsoventral regionalization described in the spinal cord and hindbrain (reviews in Ju et al. [2004]; Puelles [2013]; see also sources cited therein), it is accepted that there are 5 dorsoventral microzones in the basal plate and 6–8 microzones in the alar plate [Briscoe et al., 1999; Gray, 2013]. The classic cytoarchitectonic division of the spinal cord only contemplates ventral, lateral, and dorsal horns, with the possible addition of Clarke's thoracic column, a structural schema that clearly falls short of the richer molecular background (11–13 microzones). It is conventionally concluded by those studying spinal molecular microzones that *different types* of neurons are produced in each microzone. These are held to recombine secondarily in a more or less layered pattern within the mantle to configurate the dorsal, lateral, and ventral horns (Cajal already described early spinal alar neurons migrating into the basal plate, and some basal preganglionic neurons also migrate tangentially into the alar lateral horn) [Levi-Montalcini, 1950; Yip et al., 2000; Puelles, 2009]. The basal microzonal pattern of histogenesis would generate the diverse interneuronal cell types mixed with somatic motoneurons in the ventral horn. Analogous mechanisms would operate in the hindbrain, where diverse sensory columns are generated in the alar plate, whereas the diverse somatic, preganglionic, and branchiomotor neuronal cell types jointly with assorted reticular cell types come to occupy stereotypic positions at each neuromeric level. Interestingly, the 6–8 alar spinal and hindbrain microzones have been ascribed to two molecularly characteristic neuronal groups (microzones D1–D3 forming A-type cells and microzones D4–D6 forming B-type cells) [Storm et al., 2009]; these two major cell groupings possibly correlate

with our DL and D histogenetic zones (full review in Puelles [2013]).

It is of interest that our AChE approach in the chick hindbrain does not detect 6 different columns of alar postmitotic cells at any time. We see instead distinct *dorsolateral* and *dorsal* differentiating mantle zones extending rather homogeneously across all rhombomeres where alar neurons (plus immigrated basal motoneurons) accumulate. This maybe reflects in some way the simpler dorsal horn pattern of the spinal cord (where less sensory modalities are analyzed), implying initial formation of primordial sensory columnar *pronuclei* which later subdivide or differentiate into the known adult brainstem sensory columns. This occurs possibly in relation both to activation of given differentiation genes and the molecularly guided arrival of different trigeminal, viscerosensory, vestibular, and cochlear afferent tracts.

Comparison of the AChE-positive V, VL, DL, and D zones with the identically named *cytoarchitectonic* proto-columns identified by Hugosson [1957] at somewhat later stages (stages HH23–30 in the chick), suggests that our approach captures the earlier stages of these phenomena, which Hugosson [1957] apparently could not identify in his hematoxylin preparations. However, his material does suggest that our four early histogenetic zones are the definitive ones. He also identified that these zones show early on *proliferative maxima* (measured as number of mitoses per unit of related ventricular zone volume; see his Fig. 4–7). Interestingly, he also registered a gap between VL and DL that coincides with the gap observed by us, which showed *reduced proliferation* (his Fig. 4). As commented above, the histogenetic process probably continues after the last stage studied by us, eventually adding cells that finally fill the cell-poor alar-basal boundary gap identified between the main basal and alar cell aggregations. More detailed AChE studies in sectioned material in combination with genes characteristic of each sensory column are needed to study this issue in more detail.

We accordingly must expect that particular genes will be involved in controlling differential neurogenetic phenomena in all brain sites. This may occur independently in *each neuromere* and *even in each AP or DV intraneuromeric microzonal subdivision*. A different issue is how the diversity of neuronal types generated in such microzonal patterns combines in the alar mantle to build complex, often layered, sensory or other analytic formations. Probably differential adhesive properties coded by the microzonal molecular profiles are relevant in the histogenetic stage that precedes synaptogenesis [Redies, 2000; Redies and Puelles, 2001; Hirano et al., 2003]. This is ir-

respective that given genes are actually *shared* along a series of microzones or neuromeres forming a plurisegmental columnar pattern; such genes presumably participate combinatorially with other genes in *differential molecular profiles* characteristic of each successive neuromere, subdomain, or microzone of the complex. Sharedness or partial similarity of molecular pattern apparently correlates with similarity of *histogenetic type*, a feature typical of sensory columns distributed over a series of neuromeres, and probably with other properties as well (e.g., connectivity).

Of course, *neurogenetic events* are complex sequential phenomena involving both progenitor and daughter cells, and their environment. They must be controlled by multiple molecular circumstances, including a variety of enhancer and repressor genomic effects. Thus, recognition of a selective gene expression pattern that correlates positionally with a given emergent neuronal population does not provide a full explanation of its development either, though it does open the way for further analysis of the underlying complexities.

#### *Comparative Considerations*

We may examine the present AChE results on lizard, chicken, and rat embryos by centering our attention on common or shared aspects between the respective neurogenetic patterns. It is not difficult to realize that differentiation of a series of specific alar and basal brain derivatives across the different neuromeric units contemplated in the prosomeric model essentially represents a largely conserved pattern across these species, irrespective of any differential (i.e., heterochronic) timing results. Much the same can be said if the comparisons are made with described neural tube neuroepithelial subdivisions in amphibian and fish anamniotes of all sorts, down to cyclostomes [e.g., Pombal et al., 2009]. This is the main reason why the prosomeric model represents a molecularly based Bauplan of brain structure in vertebrates, whose topologically conserved regionalization pattern can be expanded, adding subdivisions predicted and properly corroborated from the pattern known to exist in other species [Nieuwenhuys and Puelles, 2016].

A complementary comparative approach, particularly interesting for our present endeavor, is to concentrate on evidence of *differential* neurogenetic heterochrony across the studied species. This implies that *the same Bauplan can be constructed differently over time* in some branches of the phylogenetic tree. There is a temporal *relativity* of the Bauplan structure and units in this respect.

Indeed, our forebrain data illustrate various aspects in which the relative temporal order of *equivalent neurogenetic phenomena* is different in the chosen reptile, bird, or mammal (Fig. 16). For instance, the chicken m1 tectal alar area (tect) was distinctly retarded as a whole relative to the more progressive diencephalic alar domains (leaving apart Me5, a separate microzone). In contrast, this tect area showed relatively earlier development in lizard embryos, at stages in which the alar diencephalon was hardly populated. The rat tectal area (or collicular area) seems to accompany roughly the neighboring pretectum in its neurogenetic pattern, but is in advance of the thalamus and prethalamus, in contrast with the chick case. This tectal territory nevertheless *forms homologous final derivatives* (tectal gray, superior colliculus and inferior colliculus in mammals, readily comparable to sauropsidian counterparts), so that the observed marked interspecies heterochrony *is not a cause of differential fates*. Rather, we think that the heterochronic neurogenetic aspects observed among these three amniote species may underlie instead well-known *morphogenetic differences* that characterize the final shapes of homologous regions, leading the most retarded chicken tectum to produce the largest vesicular outgrowth (retardation of neurogenesis leads to increased surface growth), and less so in reptiles. In the case of mammals, there is hardly any vesicular outpouching of the alar midbrain at all, leading to its typical tubular aqueductal cavity.

Another clear case of heterochrony between the studied amniote species (within the same Bauplan) was noted at the alar prethalamus. In the lizard, its population increases rapidly in advance of the thalamus and pretectum (Fig. 7). In the chick, the alar prethalamus is retarded compared with the thalamus and pretectum. In the rat, the pretectum is the most progressive diencephalic alar territory, and the prethalamus seems the most retarded. We had noted before that in advanced lizard embryos the prethalamus is significantly larger than the thalamus in sagittal sections (about double as long along the prosomeric axis), whereas in the mouse the thalamus is about double as long as the prethalamus [see Puelles et al., 2012a; their Fig. 8.13]. These relative size differences must be consequent to developmental proliferative heterochrony correlated inversely with the neurogenetic patterns (i.e., early differentiating areas stay small, whereas late differentiating ones contain finally more cells).

One thinks, moreover, that the particularly large mammalian thalamus probably correlates with the relatively large mammalian cortex, whereas the smaller reptilian thalamus possibly correlates with the minor size of

the corresponding homolog pallial domain (this is relatively small in reptiles and birds) [see Puelles et al., 2017]. These reflections lead to the idea that the role of interspecies evolutionary variation in the chronological pattern of proliferative and neurogenetic phenomena (heterochrony) possibly is *to mould the species-specific morphogenesis and final shape of given brain parts*, rather than affect the relative *position, boundaries*, molecular identities, and *fates* of the different brain morphogenetic units [Nieuwenhuys and Puelles, 2016]. The implied inherited *deep sameness* irrespective of variations in size, form, connections, and functions must underpin our thinking on homology.

### Evidence of Tangential Migrations

Though our approach in these studies is the description of fixed tissue, it is remarkable that the conjunction of discriminative staining and closely sampled stages with a precise prosomeric approach to positional mapping (in terms of identifying precisely the different places where *the same cells* may be found) did suggest in various instances the possibility of little known tangential neuronal migrations.

We commented in Results about the apparent rostro-caudal migration of a contingent of Me5 cells from the midbrain into the prepontine alar hindbrain; this migration seems restricted to mammals and occurs along the descending me5 tract. In adult rodents, many Me5 neurons are observed laterally to the locus coeruleus, which extends across r1 and r0 (the isthmocerebellar prepontine domain, selectively subject to isthmic secondary organizer signals). Another species difference relative to this population is that it visibly emerges at or next to the roofplate in lizard and chick embryos (where no analogous caudalward migration occurs), but not so in the rat [Puelles et al., 2015a]. As far as we could detect, Me5 cells first appear as AChE-positive elements in rat embryos at the ventrolateral rim of the alar m1 domain already at E11 (see Fig. 10b). This ventrolateral site is where normally in birds the initially dorsoventrally coursing me5 axons bend caudalwards into their descending course into the trigeminal root in r2. We speculated in Puelles et al. [2015b] that perhaps mammalian Me5 neurons do arise before E11 at the standard dorsal site of sauropsids and secondarily translocate their cell bodies ventrally to the ulterior ventrolateral position. This explanation would achieve consistency with Johnston's [1909] theory that explains this singular cell type as a misplaced neural crest derivative captured inside the midbrain during neurulation. Hodologically and functionally these neurons be-

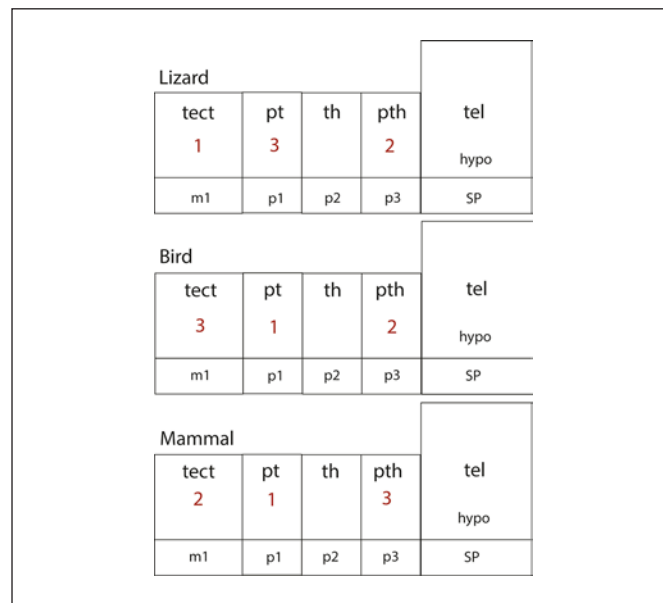


**Fig. 16.** Schemata visualizing graphically major heterochronic differences in the timing of neurogenesis in alar territories of the forebrain in the studied lizard, bird, and mammalian species. The schemata are equivalent prosomeric topological maps of the forebrain that emphasize the longitudinal and dorsoventral dimensions, and have blocks representing the midbrain (m1), the diencephalon (p1–p3), and the secondary prosencephalon (SP). The major histogenetic areas compared are identified at the top (tect, pt, th, pth). The large red numbers centered in these areas indicate the relative temporal order in which the areas start to produce neurons in each species (1 being the earliest and 3 the latest). Note each of the three species has a different heterochronic pattern in this particular aspect. Similar comparisons can be made point to point across many other brain regions (see other Figures).

have as sensory ganglion cells, and sometimes they are accompanied by melanocytes, another type of neural crest derivative [Puelles and Gil, 1978].

Our material also provided images over chicken stages 19–21 consistent with the well-known migratory crossing of the hindbrain floorplate at r4 level by a specific group of neurons representing magnocellular vestibular efferent cells, whose resulting crossed axons project peripherally through the vestibular nerve root [Simon and Lumsden, 1993].

Finally, our detailed hindbrain material in the chick allows us to corroborate previous findings about a lateralward (dorsalward) tangential somatic translocation of early-born basal branchiomotor and preganglionic neurons of the mixed cranial nerves. This displacement is preceded by the outgrowth of the corresponding axons into the “door” opened in the alar plate by incoming gan-

glionic sensory fibers [Heaton and Moody, 1980; Moody and Heaton, 1983a,b]. Classic studies including neurofibrillary analysis by Windle and Austin [1936] in the chick had previously discovered the progressive lateral displacement of the visceromotor efferent neurons; these were believed to stop within the intermediomedial column of the basal plate, due to the false assumption that all motoneurons lie in the adult basal plate. However, Ju et al. [2004] examined this point in the light of molecular markers of the alar-basal boundary, finding that the migrating branchiomotor neurons (as well as the accompanying parasympathetic preganglionic neurons) actually enter the nearest part of the alar plate and become stabilized there, close to the nerve root where they had introduced initially their axons. Except in birds, the facial nucleus branchial motoneurons of tetrapods oddly first migrate in paramedian position from r4 into r6, and only then proceed to their approach of the local alar plate site where they are found in the adult r6 (see migr7 in our Fig. 10a; in birds, which apparently lost evolutionarily this r4-into-r6 migration, the facial nucleus forms instead in alar r4, thus remaining in the rhombomere where they are born). We recently tested this bird-based conclusion of Ju et al. [2004] in the mouse, using a transgenic Pax7-LacZ line in which only alar neurons are labelled [Puelles et al., 2019b]. It was found that the unlabelled (basal) branchiomotor nuclei clearly get placed secondarily inside the labelled alar plate domain. This basal-into-alar motoneuronal migration also seems discernible in our chick flattened hindbrain wholemount material at least for the larger trigeminal and facial elements; we apparently visualize this migration at slightly earlier stages than did Ju et al. [2004] employing the *Phox2b* marker.

## References

- Albuixech-Crespo B, López-Blanch L, Burguera D, Maeso I, Sánchez-Arrones L, Moreno-Bravo JA, et al. Molecular regionalization of the developing *Amphioxus* neural tube challenges major partitions of the vertebrate brain. *PLoS Biol.* 2017 Apr 19;15(4):e2001573.
- Alonso A, Merchán P, Sandoval JE, Sánchez-Arrones L, García-Cazorla A, Artuch R, et al. Development of the serotonergic cells in murine raphe nuclei and their relations with rhombomeric domains. *Brain Struct Funct.* 2012;218:1229–77.
- Altman J, Bayer SA. Development of the diencephalon in the rat. I. Autoradiographic study of the time of origin and settling patterns of neurons of the hypothalamus. *J Comp Neurol.* 1978;182:945–71.
- Altman J, Bayer SA. The development of the rat hypothalamus. *Adv Anat Embryol Cell Biol.* 1986;100:1–178.
- Altman J, Bayer SA. Development of the rat thalamus. I. Mosaic organization of the thalamic neuroepithelium. *J Comp Neurol.* 1988;275:346–77.
- Altman J, Bayer SA. *Atlas of prenatal rat brain development.* Boca Raton, FL, USA: CRC Press, Inc; 1995.
- Amat JA. *Compartimentación y dinámica neurogenética del tubo neural del embrión de pollo. Manifestación heterocronica del plan estructural del neuroeje:* Doctoral thesis Univ.Murcia; 1986.
- Angevine JBJr. Time of neuron origin in the diencephalon of the mouse: an autoradiographic study. *J Comp Neurol.* 1970;139:129–87.

## Statement of Ethics

All experimental protocols and handling, use, and care of laboratory animals were conducted in compliance with the current normative standards of the European Union (Directive 2010/63/EU), the Spanish Government (Royal Decree 1201/2005 and 53/2013; Law 32/107), and had the approval of the University of Murcia committee for animal experimental ethics (No. A13170406). No human material was used.

## Conflict of Interest Statement

The authors have no conflicts of interest to declare.

## Funding Sources

The support of the Spanish Ministry of Economy and Competitiveness grant BFU2014-57516P (with European Community FEDER support), and a Seneca Foundation (Autonomous Community of Murcia) Excellency Research contract, reference: 19904/GERM/15; project name: Genoarchitectonic Brain Development and Applications to Neurodegenerative Diseases and Cancer (to Luis Puelles), by Seneca Foundation (5672 Fundación Séneca) are acknowledged. University of Murcia, VAT: ESQ3018001B.

## Author Contributions

Margaret Martínez-de-la-Torre, Bárbara Fernández, Carmen Maria Trujillo, José A. Amat, and Luis Puelles contributed to obtainment of specimens, AChE-histochemical processing and subsequent dissection, analysis, and photography. Luis Puelles conceived the project and wrote with José A. Amat the manuscript. All authors approved the final version of the manuscript.

## Data Availability Statement

All data analyzed during this study are included in this article. Further enquiries can be directed to the corresponding author.

- Bardet SM, Ferran JL, Sanchez-Arrones L, Puelles L. Development of *Shh* expression at the chicken telencephalic stalk. *Front Neuroanat*. 2010;4:1–16.
- Bayer SA, Altman J. *Neocortical development*. New York: Raven Press; 1991.
- Bergquist H, Kallen B. Studies on the topography of the migration areas in the vertebrate brain. *Acta Anat*. 1953;17:353–69.
- Bergquist H, Kallen B. Notes on the early histogenesis and morphogenesis of the central nervous system in vertebrates. *J Comp Neurol*. 1954;100:627–59.
- Briscoe J, Sussel L, Serup P, Hartigan-O'Connor D, Jessell TM, Rubenstein JLR, et al. Homeobox gene *Nkx2.2* and specification of neuronal identity by graded Sonic hedgehog signaling. *Nature*. 1999;398:622–7.
- Bulfone A, Puelles L, Porteus MH, Frohman MA, Martin GR, Rubenstein JLR. Spatially restricted expression of *Dlx-1*, *Dlx-2 (Tes-1)*, *Gbx-2* and *Wnt-3* in the embryonic day 12.5 mouse forebrain defines potential transverse and longitudinal segmental boundaries. *J Neurosci*. 1993;13:3155–72.
- Bulfone A, Smiga SM, Shimamura K, Peterson A, Puelles L, Rubenstein JLR. T-Brain-1 (*Tbr-1*): a homologue of *Brachyury* whose expression defines molecularly distinct domains within the cerebral cortex. *Neuron*. 1995;15:63–78.
- Cambroner F, Puelles L. Rostrocaudal nuclear relationships in the avian medulla oblongata: Fate-map with quail-chick chimeras. *J Comp Neurol*. 2000;427:522–45.
- Cobos I, Shimamura K, Rubenstein JL, Martínez S, Puelles L. Fate map of the avian anterior forebrain at the four-somite stage, based on the analysis of quail-chick chimeras. *Dev Biol*. 2001;239:46–67.
- Coggeshall RE. A study of diencephalic development in the albino rat. *J Comp Neurol*. 1964;122:241–69.
- Creps ES. Time of neuro origin in preoptic and septal areas of the mouse: an autoradiographic study. *J Comp Neurol*. 1974;157:161–244.
- Dávila JC, Guirado S, Puelles L. Calcium-binding proteins in the diencephalon of the lizard *Psammotromus algirus*. *J Comp Neurol*. 2000;427:67–92.
- Díaz C, Puelles L. Developmental genes and malformations in the hypothalamus. *Front Neuroanat*. 2020;14:1–28.
- Díaz C., Yanes C., Trujillo C.Ma., Puelles L. The lacertidian reticular thalamic nucleus projects topographically upon the dorsal thalamus: Experimental study in *Gallotia galloti*. 343: 193-208/1994. *Journal of Comparative Neurology*. 1994;343:193–208.
- Dufaure JP, Hubert J. Tables de développement du lézard vivipare: *Lacerta vivipara*. *Arch Anat Microsc Morphol Exp*. 1961;50:309–27.
- Ferran JL, Sánchez-Arrones L, Sandoval JE, Puelles L. A model of early molecular regionalization in the chicken embryonic pretectum. *J Comp Neurol*. 2007;505:379–403.
- Ferran JL, Sánchez-Arrones L, Bardet SM, Sandoval JE, Martínez-de-la-Torre M, Puelles L. Early pretectal gene expression pattern shows a conserved anteroposterior tripartition in mouse and chicken. *Brain Res Bull*. 2008;75:295–8.
- Ferrán JL, Dutra de Oliveira E, Sánchez-Arrones L, Sandoval JE, Martínez-de-la-Torre M, Puelles L. Genoarchitectonic profile of developing nuclear groups in the chicken pretectum. *J Comp Neurol*. 2009;517:405–51.
- Ferran JL, Puelles L, Rubenstein JLR. Molecular codes defining rostrocaudal domains in the embryonic mouse hypothalamus. In: Alvarez-Bolado G, Grinevich V, Puelles L, editors. *Development of the hypothalamus*. Lausanne: Frontiers Media; 2015.
- Fritzsche B, Christensen MA, Nichols DH. Fiber pathways and positional changes in efferent perikarya of 2.5- to 7-day chick embryos as revealed with DiI and dextran amines. *J Neurobiol*. 1993;24:1481–99.
- García-Calero E, López-González L, Martínez-de-la-Torre M, Fan C-M, Puelles L. Sim1-expressing cells illuminate the origin and course of migration of the nucleus of the lateral olfactory tract in the mouse amygdala. *Brain Struct Funct*. 2021 Mar;226(2):519–62.
- García-Calero E, Martínez-de-la-Torre M, Puelles L. The avian griseum tectale: cytoarchitecture, NOS expression and neurogenesis. *Brain Res Bull*. 2002;57:353–8.
- García-Calero E, Fernández-Garre P, Martínez S, Puelles L. Early mamillary pouch specification in the course of prechordal ventralization of the forebrain tegmentum. *Devel Biol*. 2008;320:366–77.
- González G, Puelles L, Medina L. Organization of the mouse dorsal thalamus based on topology, calretinin immunostaining and gene expressions. *Brain Res Bull*. 2002;57:439–43.
- Gray PA. Transcription factors define the neuroanatomical organization of the medullary reticular formation. *Front Neuroanat*. 2013;7:7.
- Gribnau AA, Geijsberts LG. Morphogenesis of the brain in staged Rhesus monkey embryos. *Adv Anat Embryol Cell Biol*. 1985;91:1–69.
- Hamburger V, Hamilton HL. A series of normal stages in the development of the chick embryo. *J Morphol*. 1951;88(1):49–92.
- Heaton MB, Moody SA. Early development and migration of the trigeminal motor nucleus in the chick embryo. *J Comp Neurol*. 1980;189:61–99.
- Herrick CJ. The morphology of the forebrain in amphibia and reptilia. *J Comp Neurol Psychol*. 1910;20(5):413–547.
- Herrick CJ. Morphogenesis of the brain. *J Morphol*. 1933;54(2):233–58.
- Herrick CJ. *The brain of the tiger salamander, *Amblystoma tigrinum**. Chicago: The University of Chicago Press; 1948.
- Hidalgo-Sánchez M, Martínez-de-la-Torre M, Alvarado-Mallart RM, Puelles L. Distinct pre-isthmus domain defined by overlap of *Otx2* and *Pax2* expression domains in the chicken caudal midbrain. *J Comp Neurol*. 2005;483:17–29.
- Hirano S, Suzuki ST, Redies C. The cadherin superfamily in neural development: diversity, function, and interaction with other molecules. *Front Biosci*. 2003;8:306–55.
- His W. Vorschläge zur eintheilung des gehirns. *Arch Anat Physiol Anat Abt*. 1893:172–80.
- His W. Die anatomische nomenclatur. Nomina anatomica. *Arch Anat Entwickl Gesch*. 1895;1895(Suppl):1–180.
- His W. *Die entwicklung des menschlichen gehirns während der ersten monate*. Leipzig: S: Hirzel Verlag; 1904.
- Hugosson R. *Morphologic and experimental studies on the development and significance of the rhombencephalic longitudinal columns*. Lund: Hakan Ohlssons Boktryckeri; 1957.
- Johnston JB. The radix mesencephalica trigemini. *J Comp Neurol Psychol*. 1909;19(6):593–644.
- Ju MJ, Aroca P, Luo J, Puelles L, Redies C. Molecular profiling indicates avian branchiomotor nuclei invade the hindbrain alar plate. *Neuroscience*. 2004;128:785–96.
- Karnovsky MJ, Roots L. A “direct-coloring” thiocholine method for cholinesterases. *J Histochem Cytochem*. 1964;12:2019–221.
- Keyser A. The development of the diencephalon of the Chinese hamster. An investigation of the validity of the criteria of subdivision of the brain. *Acta Anat Suppl*. 1972;59:1–178.
- Kuhlenbeck H. Part II: overall morphological pattern. In: *The central nervous system of vertebrates*. Basel, Switzerland: Karger; 1973. Vol. 3.
- LaVail JH, Cowan WM. The development of the chick optic tectum. II. Autoradiographic studies. *Brain Res*. 1971;28:421–41.
- Levi-Montalcini R. The origin and development of the visceral in the spinal cord of the chick embryo. *J Morphol*. 1950;86(2):253–83.
- Marín F, Puelles L. Morphological fate of rhombomeres in quail/chick chimeras: a segmental analysis of hindbrain nuclei. *Eur J Neurosci*. 1995;7:1714–38.
- Marín F, Aroca P, Puelles L. Hox gene colinear expression in the avian medulla oblongata is correlated with pseudorhombomeric domains. *Devel Biol*. 2008;323:230–47.
- Martínez S, Alvarado-Mallart RM, Martínez de la Torre M, Puelles L. Retinal and tectal connections of embryonic nucleus superficialis magnocellularis and its mature derivatives in the chick. *Anat Embryol*. 1991;183:235–43.
- Martínez S, Puelles E, Puelles L, Echevarría D. Molecular regionalization of the developing neural tube. In: Watson C, Paxinos G, Puelles L, editors. *The mouse nervous system*: Academic Press/Elsevier; 2012. p. 2–18.
- Martínez-de-la-Torre M. *Estructura del mesencéfalo y diencefalo en aves y reptiles: aportaciones a una síntesis en la búsqueda de homologías – doctoral thesis*. Univ.Murcia; 1985.
- Martínez de la Torre M, Martínez S, Puelles L. Solitary magnocellular neurons in the avian optic tectum: cytoarchitectonic, histochemical and (3H) thymidine autoradiographic characterization. *Neurosci Lett*. 1987;74:31–6.

- Martínez-de-la-Torre M, Garda AL, Puelles E, Puelles L. *Gbx2* expression in the late embryonic chick dorsal thalamus. *Brain Res Bull.* 2002;57:435–8.
- Medina L, Martí E, Artero C, Fasolo A, Puelles L. Distribution of neuropeptide Y-like immunoreactivity in the brain of the lizard *Gallotia galloti*. *J Comp Neurol.* 1992;319:387–405.
- Medina L, Smeets WJ, Hoogland PV, Puelles L. Distribution of choline acetyltransferase immunoreactivity in the brain of the lizard *Gallotia galloti*. *J Comp Neurol.* 1993;331:261–85.
- Moody SA, Heaton MB. Developmental relationships between trigeminal ganglia and trigeminal motoneurons in chick embryos: I. Ganglion development is necessary for motoneuron migration. *J Comp Neurol.* 1983a;213:327–43.
- Moody SA, Heaton MB. Developmental relationships between trigeminal ganglia and trigeminal motoneurons in chick embryos: II. Ganglion axon ingrowth guides motoneuron migration. *J Comp Neurol.* 1983b;213:344–9.
- Nieuwenhuys R. Principles of current vertebrate neuromorphology. *Brain Behav Evol.* 2017;90(2):117–30.
- Nieuwenhuys R, Puelles L. *Towards a new neuro-morphology*. Berlin: Springer Verlag; 2016.
- Orr H. Contribution to the embryology of the lizard; with especial reference to the central nervous system and some organs of the head; together with observations on the origin of the vertebrates. *J Morphol.* 1887;1(2):311–72.
- Palmgren A. Embryological and morphological studies on the mid-brain and cerebellum of vertebrates. *Acta Zool.* 1921;2(1–2):1–94.
- Pombal MA, Megias M, Bardet SM, Puelles L. New and old thoughts on the segmental organization of the forebrain in lampreys. *Brain Behav Evol.* 2009;74:7–19.
- Prada C, Puelles L, Génis-Gálvez JM. A Golgi study on the early sequence of differentiation of ganglion cells in the chick embryo retina. *Anat Embryol.* 1981;161:305–17.
- Puelles L. A segmental morphological paradigm for understanding vertebrate forebrains. *Brain Behav Evol.* 1995;46:319–37.
- Puelles L. Brain segmentation and forebrain development in amniotes. *Brain Res Bull.* 2001;55:695–710.
- Puelles L. Contributions to neuroembryology of Santiago Ramon y Cajal (1852–1934) and Jorge F. Tello (1880–1958). *Int J Dev Biol.* 2009;53:1145–60.
- Puelles L. Plan of the developing vertebrate nervous system relating embryology to the adult nervous system (prosomere model, overview of brain organization). In: Rubenstein JLR, Rakic P, editors. *Comprehensive developmental neuroscience: patterning and cell type specification in the developing CNS and PNS*. Amsterdam: Academic Press; 2013. Vol.2. p. 187–209.
- Puelles L. Role of secondary organizers in the evolution of forebrain development in vertebrates. In: Shepherd SV, editor. *Chapter in handbook of evolutionary neuroscience*. Chichester, UK: Blackwell-Wiley; 2017. p. 350–87.
- Puelles L. Developmental studies of avian brain organization. *Int J Dev Biol.* 2018;62:207–24.
- Puelles L. Survey of midbrain, diencephalon, and hypothalamus neuroanatomic terms whose prosomeric definition conflicts with columnar tradition. *Front Neuroanat.* 2019;13:20.
- Puelles L, Amat JA, Martínez-de-la-Torre M. Segment-related, mosaic neurogenetic pattern in the forebrain and mesencephalon of early chick embryos. I. Topography of AChE-positive neuroblasts up to stage HH18. *J Comp Neurol.* 1987a;266:147–268.
- Puelles L, Diaz C, Stühmer T, Ferran JL, Martínez-de la Torre M, Rubenstein JLR. LacZ-reporter mapping of *Dlx5/6* expression and genoarchitectural analysis of the postnatal mouse prethalamus. *J Comp Neurol.* 2021. Online ahead of print.
- Puelles L, Domenech-Ratto G, Martínez-de-la-Torre M. Location of the rostral end of the longitudinal brain axis: review of an old topic in the light of marking experiments on the closing rostral neuropore. *J Morphol.* 1987b;194:163–71.
- Puelles L, Fernández B, Martínez-De-La-Torre M. Neuromeric landmarks in the rat mid-brain, diencephalon and hypothalamus, compared with acetylcholinesterase histochemistry. 4th edn. In: Paxinos G, editor. *The rat nervous system*. New York: Academic Press/Elsevier; 2015a. p. 25–43.
- Puelles L, Guillén M, Martínez de la Torre M. Observations on the fate of nucleus superficialis magnocellularis of Rendahl in the avian diencephalon, bearing on the organization and nomenclature of neighboring retinorecipient nuclei. *Anat Embryol.* 1991;183:221–33.
- Puelles L, Gil M. Diferenciación transitoria de melanocitos en el techo del istmo tronco encefálico en embriones de pollo. *Anales del Desarrollo.* 1978;22/52:3–7.
- Puelles L, Harrison M, Paxinos G, Watson C. A developmental ontology for the mammalian brain based on the prosomeric model. *Trends Neurosci.* 2013;36:570–8.
- Puelles L, Kuwana E, Puelles E, Keleher J, Bulfone A, Rubenstein JLR. Pallial and subpallial derivatives in the chick and mouse telencephalon, traced by the embryonic expression profiles of the genes *Dlx-2*, *Emx-1*, *Nkx-2.1*, *Pax-6* and *Tbr-1*. *J Comp Neurol.* 2000;424:409–38.
- Puelles L, Martínez S, Martínez-de-la-Torre M, Rubenstein JLR. Gene maps and related histogenetic domains in the forebrain and mid-brain. 3rd edn. In: Paxinos G., editor. *The rat nervous system*. San Diego, CA, USA: Academic Press; 2004. p. 3–25.
- Puelles L, Martínez S, Martínez-De-La-Torre M, Rubenstein JLR. Gene maps and related histogenetic domains in the forebrain and mid-brain. 4th edition. In: Paxinos G, editor. *The rat nervous system*. New York: Academic Press/Elsevier; 2015b. p. 3–24.
- Puelles L, Martínez-de-la-Torre M. Autoradiographic and Golgi study on the early development of n. isthmi principalis and adjacent grisea in the chick embryo: a tridimensional viewpoint. *Anat Embryol.* 1987;176:19–34.
- Puelles L, Martínez-de-la-Torre M, Bardet S, Rubenstein JLR. Hypothalamus. In: Watson C, Paxinos G, Puelles L, editors. *The mouse nervous system*. Academic Press/Elsevier; 2012a. p. 221–312.
- Puelles L, Martínez-de-la-Torre M, Martínez S, Watson C, Paxinos G. *The chick brain in stereotaxic coordinates and alternate stains*. 2nd edn. New York: Academic Press; 2019a.
- Puelles E, Martínez-de-la-Torre M, Watson C, Puelles L. Midbrain. In: Watson C, Paxinos G, Puelles L, editors. *The mouse nervous system*. Academic Press/Elsevier; 2012b. p. 337–59.
- Puelles L, Rubenstein JL. Expression patterns of homeobox and other putative regulatory genes in the embryonic mouse forebrain suggest a neuromeric organization. *Trends Neurosci.* 1993;16:472–9.
- Puelles L, Rubenstein JL. Forebrain gene expression domains and the evolving prosomeric model. *Trends Neurosci.* 2003;26:469–76.
- Puelles L, Rubenstein JLR. A new scenario of hypothalamic organization: rationale of new hypotheses introduced in the updated prosomeric model. In: Alvarez-Bolado G, Grinevich V, Puelles L, editors. *Development of the hypothalamus*. Lausanne: Front Neuroanat; 2015. Vol. 9; p. 83.
- Puelles L, Robles C, Martínez de la Torre M, Martínez S. New subdivision schema for the avian torus semicircularis: neurochemical maps in the chick. *J Comp Neurol.* 1994;340:98–125.
- Puelles L, Sandoval JE, Ayad A, del Corral R, Alonso A, Ferran JL, et al. The pallium in reptiles and birds in the light of the updated tetrapartite pallium model. In: Kaas J, editor. *Evolution of nervous systems*. Oxford: Elsevier; 2017. 1. p. 519–55.
- Puelles L, Tvrdik P, Martínez-de-la-Torre M. The postmigratory alar topography of visceral cranial nerve efferents challenges the classical model of hindbrain columns. *Anat Rec.* 2019b;302:485–504.
- Ramos A. *Tabla de desarrollo embrionario de *Lacerta Gallotia galloti* (periodo de embriogénesis) y aspectos de su reproducción*. Canary Islands, Spain: Memoria de Licenciatura. Universidad de La Laguna; 1992.
- Redies C. Cadherins in the central nervous system. *Prog Neurobiol.* 2000;61(6):611–48.
- Redies C, Puelles L. Modularity in vertebrate brain development and evolution. *Bioessays.* 2001;23:1100–11.
- Redies C, Ast M, Nakagawa S, Takeichi M, Martínez-de-la-Torre M, Puelles L. Morphologic fate of diencephalic prosomeres and their subdivisions revealed by mapping cadherin expression. *J Comp Neurol.* 2000;421:481–514.
- Rendahl H. Embryologische und morphologische studien über das zwischenhirn beim huhn. *Acata Zool.* 1924;5(1–2):241–344.

- Rubenstein JL, Martinez S, Shimamura K, Puelles L. The embryonic vertebrate forebrain: the prosomeric model. *Science*. 1994;266:578–80.
- Shimamura K, Hartigan DJ, Martinez S, Puelles L, Rubenstein JL. Longitudinal organization of the anterior neural plate and neural tube. *Development*. 1995;121:3923–33.
- Simon H, Lumsden A. Rhombomere-specific origin of the contralateral vestibulo-acoustic efferent neurons and their migration across the embryonic midline. *Neuron*. 1993;11:209–20.
- Storm R, Cholewa-Waclaw J, Reuter K, Bröhl D, Sieber M, Treier M, et al. The bHLH transcription factor *Olig3* marks the dorsal neuroepithelium of the hindbrain and is essential for the development of brainstem nuclei. *Development*. 2009;136:295–305.
- Studer M. Initiation of facial motoneurone migration is dependent on rhombomeres 5 and 6. *Development*. 2001;128:3707–16.
- Swanson LW. *Brain architecture. Understanding the basic plan*. 2nd edn. Oxford: Oxford Univ. Press; 2012.
- Tiveron MC, Pattyn A, Hirsch MR, Brunet JF. Role of *Phox2b* and *Mash1* in the generation of the vestibular efferent nucleus. *Dev Biol*. 2003;260:46–57.
- Tomás-Roca L, Corral-San-Miguel R, Aroca P, Puelles L, Marín F. Crypto-rhombomeres of the mouse medulla oblongata, defined by molecular and morphological features. *Brain Struct Funct*. 2016;221:815–38.
- Vaage S. The segmentation of the primitive neural tube in chick embryos (*Gallus domesticus*). *Erg Anat Entwickl Gesch*. 1969;41:1–88.
- Vaage S. The histogenesis of the isthmic nuclei in chick embryos (*Gallus domesticus*). I. A morphological study. *Z Anat Entwicklungsgesch*. 1973;142:283–314.
- von Kupffer K. Die morphogenie des centralnervensystems. In: Hertwig O, editor. *Handbuch der vergleichenden und experimentellen Entwicklungslehre der Wirbelthiere*. Jena, Germany: Fischer; 1906. 2. p. 1–119.
- Windle WF, Austin MF. Neurofibrillar development in the central nervous system of chick embryos up to 5 days' incubation. *J. Comp Neurol*. 1936;63(3):431–63.
- Yip JW, Yip YP, Nakajima K, Capriotti C. Reelin controls position of autonomic neurons in the spinal cord. *Proc Natl Acad Sci U S A*. 2000; 97:8612–6.
- Yoon MS, Puelles L, Redies C. Formation of cadherin-expressing brain nuclei in diencephalic alar plate divisions. *J Comp Neurol*. 2000;427: 461–80.